

# Optimization of the Energy-Efficient Relay-Based massive IoT Network

Tiejun Lv, *Senior Member, IEEE*, Zhipeng Lin, *Student Member, IEEE*, Pingmu Huang, and Jie Zeng, *Senior Member, IEEE*

**Abstract**—To meet the requirements of high energy efficiency (EE) and large system capacity for the fifth-generation (5G) Internet of Things (IoT), the use of massive multiple-input multiple-output (MIMO) technology has been launched in the massive IoT (mIoT) network, where a large number of devices are connected and scheduled simultaneously. This paper considers the energy-efficient design of a multi-pair decode-and-forward relay-based IoT network, in which multiple sources simultaneously transmit their information to the corresponding destinations via a relay equipped with a large array. In order to obtain an accurate yet tractable expression of the EE, firstly, a closed-form expression of the EE is derived under an idealized simplifying assumption, in which the location of each device is known by the network. Then, an exact integral-based expression of the EE is derived under the assumption that the devices are randomly scattered following a uniform distribution and transmit power of the relay is equally shared among the destination devices. Furthermore, a simple yet efficient lower bound of the EE is obtained. Based on this, finally, a low-complexity energy-efficient resource allocation strategy of the mIoT network is proposed under the specific quality-of-service (QoS) constraint. The proposed strategy determines the near-optimal number of relay antennas, the near-optimal transmit power at the relay and near-optimal density of active mIoT device pairs in a given coverage area. Numerical results demonstrate the accuracy of the performance analysis and the efficiency of the proposed algorithms.

**Index Terms**—Energy efficiency, resource allocation, massive MIMO, decode-and-forward relay, green mIoT.

## I. INTRODUCTION

Internet of Things (IoT), an emerging technology attracting significant attention, promotes a heightened level of awareness about our world and has been used in various areas, such as governments, industry, and academia [1], [2]. In IoT, not only are various things (e.g., sensor devices and cloud computing systems) with substantial energy consumption, but also the connection of things (e.g., radio frequency identification (RFID) and fifth-generation (5G) network) and the interaction of things (e.g., data sensing and communications) are consuming a large amount of energy. Improving energy efficiency (EE) has become one of the main goals and design challenges for the presented IoT networks [3]. In order to achieve the most efficient energy usage, various innovative ‘green IoT’ techniques have been developed during the last few years [4]–[6].

The financial support of the National Natural Science Foundation of China (NSFC) (Grant No. 61671072) is gratefully acknowledged.

T. Lv, Z. Lin, P. Huang, and J. Zeng are with the School of Information and Communication Engineering, Beijing University of Posts and Telecommunications, Beijing 100876, China (e-mail: {lvtejun, linzlp, pmhuang, zengjie}@bupt.edu.cn).

On the other hand, connectivity is the foundation for a IoT network. It is envisioned that billions of devices will be connected in the 5G IoT network by 2020 to build a smart city [7], [8]. As one major segment of the IoT network, the *massive IoT (mIoT)* refers to the applications that are enabled by connecting a large number of IoT devices to an internet-enabled system [9], [10]. This network is typically used for the scenarios characterized by low power, wide coverage and strong support for devices on a massive scale, such as agriculture production detection, power utilization collection, medical monitoring and vehicle scheduling [11]–[13]. There is a target that connection density in the urban environment will be 1 million devices/km<sup>2</sup> [14], [15]. Considering the connection target and the energy limitation of mIoT networks, the massive multiple-input multiple-output (MIMO) technique (equipped with a large-scale antenna array), which can increase the network capacity 10 times or more without requiring more spectrum and simultaneously improve the EE of wireless systems on the order of 100 times [16], [17], has attracted increasing attention on utilization in mIoT networks [18]–[20]. As presented in [21], as one of the major enabling technologies for 5G wireless systems, massive MIMO systems are capable of increasing the EE by orders of magnitude compared to single-antenna systems, in particularly when combined with simultaneous scheduling of a large number of terminals (e.g., tens or hundreds) [22], [23]. Relying on a realistic power consumption model, the authors of [24] proved that the optimal system parameters are capable of maximizing the EE in multi-device massive MIMO systems. In [25], low-complexity antenna selection methods and power allocation algorithms were proposed to improve the EE of large-scale distributed antenna systems. The authors of [26] intended to optimize the global EE of the uplink and downlink of multi-cell massive MIMO. A joint pilot assignment and resource allocation strategy was studied in [27] to maximize the EE of multi-cell massive MIMO networks.

As a parallel research avenue, a relay-based mIoT network was shown to constitute a promising technique of expanding the coverage, reducing the power consumption and achieving energy-efficient transmission. In [5], by optimizing the available bandwidth of a relay-based mIoT network, the energy consumption of all the relay BSs is minimized. Similar to the observations in single-hop massive MIMO systems, it was shown in [28] that by invoking a relay equipped with a large-scale antenna array and a simple relay transceiver (e.g., linear zero-forcing (ZF) transceiver), the spectrum efficiency (SE) of a two-hop relay system becomes proportional to the number of

relay antennas. Therefore, the combination of massive MIMO and cooperative relaying constitutes an appealing option for energy-efficient mIoT networks.

When writing this paper, we find that the existing literature rarely focused on the research of the relay-based mIoT networks and that on massive MIMO aided relay systems mainly paid attention to the analysis of the SE. For instance, the asymptotic SE of massive MIMO aided relay systems was investigated in [29], while the SE of massive MIMO relay systems was studied in [30]. However, to the best of our knowledge, there are a paucity of contributions to the energy-efficient transmission and resource allocation strategies in massive MIMO relay-based mIoT systems. It is challenging to extend the existing energy-efficient designs conceived for single-hop massive MIMO systems [24], [25], [27] to the ones adopted in massive MIMO relay systems. Due to the fact that, compared to single-hop transmission schemes, both the design of the signal processing schemes used at the relay and the performance analysis of the massive MIMO relay systems are fundamentally dependent on the more complex two-hop channels. Therefore, it is important to design energy-efficient resource allocation strategy for a massive MIMO relay-based mIoT network.

Contrary to the above background, in this paper, we consider the performance analysis and energy-efficient resource allocation optimization of a massive MIMO decode-and-forward (DF) relay based mIoT network supporting multiple pairs of mobile mIoT devices. We assume that the channel state information (CSI) is estimated relying on the minimum mean-square error (MMSE) criterion, and the relay employs a low-complexity linear ZF transceiver. The main contributions of this paper are summarized as follows.

- Assuming that the location of each mobile device is known, we derive a closed-form expression of the EE in the considered mIoT network using a massive MIMO aided DF relay. Additionally, a simplified analytical expression is also derived for the special case where equal transmit power is allocated to all destination devices by the relay.
- Furthermore, assuming that the device locations follow a uniform random distribution, we derive an exact integral-based expression of the EE. However, since this expression cannot be integrated out, a simple yet efficient lower bound of the EE is also derived. The analytical results lay the foundation of predicting the EE and of understanding how it changes with respect to the transmit power, the number of relay antennas and the number of active mIoT device pairs.
- Based on the lower bound derived, we propose an energy-efficient resource allocation strategy which determines the near-optimal relay transmit power, the near-optimal number of relay antennas and the near-optimal number of active mIoT device pairs under the given quality-of-service (QoS) constraint. The original EE optimization problem relying on the exact but intractable EE expression is transformed into a problem that maximizes the lower bound of the EE. This transformation makes it feasible for us to solve the latter EE optimization

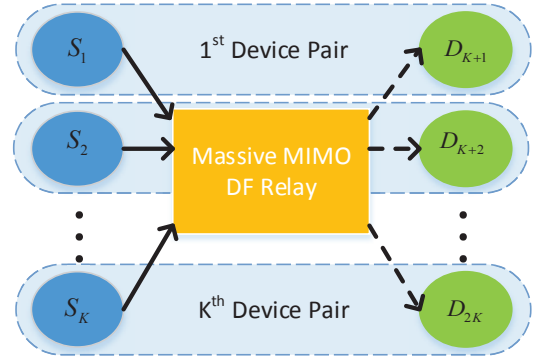


Fig. 1: The system model considered: A two-hop relay system supports  $K$  active mIoT devices communicating with their individual destination mIoT devices via a massive MIMO aided DF relay, which mitigates the inter-stream interference with a large number of antennas.

problem, which eventually gives the near-optimal system configuration of energy-efficient massive MIMO relay systems supporting multiple mIoT device pairs.

The remainder of this paper is organized as follows. Both the system model and transmission scheme of the mIoT network using the massive MIMO aided multi-pair DF relay are described in Section II. In Section III, the EE optimization problem is formulated by employing a realistic power consumption model. In Section IV, we derive the EE expressions with known device locations and uniform random distribution of device locations, respectively. Then, in Section V, an energy-efficient resource allocation strategy is proposed based on the EE expressions derived. Numerical results are provided under diverse system configurations. In Section VII, we analyze the convergence and the computational complexity of the proposed algorithms. Finally, our conclusions are drawn in Section VIII.

*Notations:* We use uppercase and lowercase boldface letters for denoting matrices and vectors, respectively.  $(\cdot)^H$ ,  $(\cdot)^T$  and  $(\cdot)^\dagger$  denote the conjugate transpose, transpose and pseudo-inverse, respectively.  $\|\cdot\|$ ,  $\text{tr}(\cdot)$ ,  $\mathbb{E}[\cdot]$  and  $\text{Var}[\cdot]$  stand for the Euclidean norm, the trace of matrices, the expectation and variance operators, respectively.  $[\mathbf{A}]_{i,j}$  represents the entry at the  $i$ -th row and the  $j$ -th column of a matrix  $\mathbf{A}$ .  $\mathcal{CN}(\mathbf{0}, \Theta)$  denotes the circularly symmetric complex Gaussian distribution with zero mean and the covariance matrix  $\Theta$ , while  $\xrightarrow{a.s.}$  denotes the *almost sure* convergence.  ${}_2F_1(\cdot)$  represents the hypergeometric function, and  $|\mathcal{A}|$  denotes the cardinality of a set  $\mathcal{A}$ . Finally,  $[\cdot]^+$  denotes  $\max\{0, \cdot\}$ .

## II. SYSTEM MODEL AND TRANSMISSION SCHEME

As shown in Fig. 1, we consider a massive MIMO aided dual-hop DF relay mIoT system supporting  $K$  pairs of single-antenna source-destination mIoT devices (i.e., active mIoT device pairs), which are selected from  $N$  pairs of candidate mIoT devices for data transmission with the aid of the  $M$ -antenna ( $K \ll M$ ) relay<sup>1</sup>. The system operates over a

<sup>1</sup>It was shown in [31] that by using simple relay transceivers (e.g., linear ZF-based transceivers), a massive MIMO relay system is capable of significantly alleviating the interference among different data streams.

bandwidth of  $B$  Hz and the channels are static within the time/frequency coherence interval of  $T = B_C T_C$  symbol duration, where  $B_C$  and  $T_C$  are the coherence bandwidth and coherence time, respectively. Particularly, each mIoT device as well as the relay uses the total bandwidth of  $B$  Hz. We focus on the active mIoT device pairs and assume that the  $k$ -th mIoT device (source node) demands to communicate with the  $(k + K)$ -th device (destination node)<sup>2</sup>. The set of active mIoT device pairs is denoted by  $\mathcal{S}$ , satisfying  $|\mathcal{S}| = K$ . The relay operates in the half-duplex time-division duplexing (TDD) mode. Each coherence interval is divided into three time phases, as shown in Fig. 2, namely the channel estimation (CE) phase, the source-to-relay transmission (S  $\rightarrow$  R) phase, and the relay-to-destination transmission (R  $\rightarrow$  D) phase.

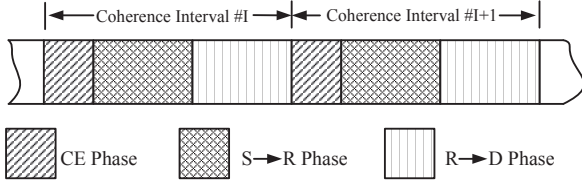


Fig. 2: Partitioning of a coherence interval.

Let  $\mathbf{G}_S = [\mathbf{g}_{S,1}, \dots, \mathbf{g}_{S,K}] \in \mathbb{C}^{M \times K}$  and  $\mathbf{G}_D = [\mathbf{g}_{D,1}, \dots, \mathbf{g}_{D,K}]^T \in \mathbb{C}^{K \times M}$  denote the channel matrices from the  $K$  active sources to the relay and from the relay to the  $K$  active destinations, respectively. The channel matrices characterize both the small-scale fading (SSF) and the large-scale fading (LSF). More precisely,  $\mathbf{G}_S$  and  $\mathbf{G}_D$  can be expressed as

$$\mathbf{G}_S = \mathbf{H}_S \mathbf{D}_S^{1/2}, \quad \mathbf{G}_D = \mathbf{D}_D^{1/2} \mathbf{H}_D, \quad (1)$$

where  $\mathbf{H}_S \in \mathbb{C}^{M \times K}$  and  $\mathbf{H}_D \in \mathbb{C}^{K \times M}$  are the SSF channel matrices and their entries are independent and identically distributed (i.i.d.) with  $\mathcal{CN}(0, 1)$ . The LSF channel matrices  $\mathbf{D}_S$  and  $\mathbf{D}_D$  are modelled as diagonal matrices with  $[\mathbf{D}_S]_{k,k} = \beta_k$  and  $[\mathbf{D}_D]_{k,k} = \beta_{k+K}$ ,  $k = 1, 2, \dots, K$ , respectively.

#### A. CE at the Relay

In the CE phase, the relay acquires the CSI of active devices by using the MMSE channel estimator given in [32]. Let  $\hat{\mathbf{G}}_S$  and  $\hat{\mathbf{G}}_D$  be the channel estimates of  $\mathbf{G}_S$  and  $\mathbf{G}_D$ , respectively. Then, we have

$$\mathbf{G}_S = \hat{\mathbf{G}}_S + \tilde{\mathbf{G}}_S, \quad \mathbf{G}_D = \hat{\mathbf{G}}_D + \tilde{\mathbf{G}}_D, \quad (2)$$

where  $\tilde{\mathbf{G}}_S$  and  $\tilde{\mathbf{G}}_D$  are the complex-valued Gaussian distributed estimation error matrices of  $\mathbf{G}_S$  and  $\mathbf{G}_D$ , respectively. According to the orthogonality principle [32],  $\hat{\mathbf{G}}_S$  and  $\tilde{\mathbf{G}}_S$  are independent of each other. Similarly,  $\hat{\mathbf{G}}_D$  and  $\tilde{\mathbf{G}}_D$  are independent of each other as well.

For the clarity of analysis, we temporarily assume that the LSF channel matrices,  $\mathbf{D}_S$  and  $\mathbf{D}_D$ , are perfectly estimated. In Section IV-B and in its subsequent sections, this assumption

<sup>2</sup>In this paper, the direct link between any source node and destination node is ignored due to large path-loss.

will then be removed. According to (2), the columns of  $\hat{\mathbf{G}}_S$ ,  $\tilde{\mathbf{G}}_S$ ,  $\hat{\mathbf{G}}_D$  and  $\tilde{\mathbf{G}}_D$  obey the distributions of

$$\begin{aligned} \hat{\mathbf{g}}_{S,k} &\sim \mathcal{CN}(\mathbf{0}, \beta'_k \mathbf{I}_M), \\ \tilde{\mathbf{g}}_{S,k} &\sim \mathcal{CN}(\mathbf{0}, \beta_k - \beta'_k \mathbf{I}_M), \\ \hat{\mathbf{g}}_{D,k} &\sim \mathcal{CN}(\mathbf{0}, \beta'_{k+K} \mathbf{I}_M), \\ \tilde{\mathbf{g}}_{D,k} &\sim \mathcal{CN}(\mathbf{0}, \beta_{k+K} - \beta'_{k+K} \mathbf{I}_M), \end{aligned} \quad (3)$$

where  $\beta'_i = \frac{\tau_r \rho_p \beta_i^2}{1 + \tau_r \rho_p \beta_i}$ ,  $i = 1, 2, \dots, 2K$ . Furthermore,  $\rho_p$  is the ratio of the transmit power of each pilot symbol to the noise power at the relay's receiver, while  $\tau_r$  ( $\tau_r \geq 2K$ ) is the pilot sequence length of each device.

#### B. Data Transmission

The relay uses the channel estimates obtained above and the low-complexity linear ZF transceivers. More specifically, the relay uses a ZF receiver to detect the signals transmitted from the  $K$  active sources, and then it uses a ZF transmit precoding scheme to forward the signals to the  $K$  active destinations.

In the S  $\rightarrow$  R phase,  $K$  sources simultaneously transmit their signals  $\mathbf{x}_d = \sqrt{P_{\text{tx,d}}}\mathbf{s} \in \mathbb{C}^{K \times 1}$  to the relay, in which  $\mathbf{s} = [s_1, \dots, s_k, \dots, s_K]^T$  is the information-bearing symbol vector satisfying  $\mathbb{E}[\mathbf{s}\mathbf{s}^H] = \mathbf{I}_K$ ,  $s_k$  is the symbol delivered from the  $k$ -th mIoT device to the relay, and  $P_{\text{tx,d}}$  is the average transmit power of each mIoT device. The signal  $\mathbf{y}_R \in \mathbb{C}^{M \times 1}$  received at the relay is given by

$$\mathbf{y}_R = \mathbf{G}_S \mathbf{x}_d + \mathbf{n}_R, \quad (4)$$

where  $\mathbf{n}_R \in \mathbb{C}^{M \times 1}$  denotes the additive white Gaussian noise (AWGN) obeying  $\mathcal{CN}(\mathbf{0}, \sigma_R^2 \mathbf{I}_M)$  at the relay.

The relay performs ZF detection relying on  $\mathbf{y}_R$ . More specifically, upon multiplying with the ZF filtering matrix  $\mathbf{F}_1 = (\hat{\mathbf{G}}_S^H \hat{\mathbf{G}}_S)^{-1} \hat{\mathbf{G}}_S^H \in \mathbb{C}^{K \times M}$ , the transmitted symbols having been superimposed over the channel are separated into  $K$  non-interfering symbols, which are denoted as  $\mathbf{x}_R \in \mathbb{C}^{K \times 1}$  and given by

$$\mathbf{x}_R = \mathbf{F}_1 \mathbf{y}_R = \mathbf{F}_1 \mathbf{G}_S \mathbf{x}_d + \mathbf{F}_1 \mathbf{n}_R. \quad (5)$$

Therefore, the  $k$ -th symbol  $x_{R,k}$  (i.e., the  $k$ -th element of  $\mathbf{x}_R$ ) is given by

$$\begin{aligned} x_{R,k} &= \sqrt{P_{\text{tx,d}}}\mathbb{E}[\mathbf{f}_{1,k}^H \mathbf{g}_{S,k}] s_k + \sqrt{P_{\text{tx,U}}}\sum_{j \neq k}^K \mathbf{f}_{1,k}^H \mathbf{g}_{S,j} s_j \\ &\quad + \sqrt{P_{\text{tx,d}}}(\mathbf{f}_{1,k}^H \mathbf{g}_{S,k} - \mathbb{E}[\mathbf{f}_{1,k}^H \mathbf{g}_{S,k}]) s_k + \mathbf{f}_{1,k}^H \mathbf{n}_R, \end{aligned} \quad (6)$$

where  $\mathbf{f}_{1,k}$  is the  $k$ -th column of  $\mathbf{F}_1$ . Then, the signal-to-interference-plus-noise ratio (SINR) of the  $k$ -th device pair in the S  $\rightarrow$  R phase is formulated as [33]

$$\begin{aligned} \gamma_k^{(1)} &= P_{\text{tx,U}} \left| \mathbb{E}[\mathbf{f}_{1,k}^H \mathbf{g}_{S,k}] \right|^2 / (P_{\text{tx,d}} \text{Var}(\mathbf{f}_{1,k}^H \mathbf{g}_{S,k}) \\ &\quad + P_{\text{tx,d}} \sum_{j \neq k}^K \mathbb{E} \left[ \left| \mathbf{f}_{1,k}^H \mathbf{g}_{S,j} \right|^2 \right] + \sigma_R^2 \mathbb{E} \left[ \left\| \mathbf{f}_{1,k} \right\|^2 \right]). \end{aligned} \quad (7)$$

During the  $R \rightarrow D$  phase, the relay decodes the information symbol vector  $\mathbf{s}$  from  $\mathbf{x}_R$  as  $\hat{\mathbf{s}} = [\hat{s}_1, \dots, \hat{s}_k, \dots, \hat{s}_K]^T$  that satisfies  $\mathbb{E}[\hat{\mathbf{s}}\hat{\mathbf{s}}^H] = \mathbf{I}_K$ , and multiplies the ZF precoding matrix of  $\mathbf{F}_2 = \hat{\mathbf{G}}_D^H (\hat{\mathbf{G}}_D \hat{\mathbf{G}}_D^H)^{-1} \in \mathbb{C}^{M \times K}$  both by the power allocation matrix at the relay and by  $\hat{\mathbf{s}}$ , yielding

$$\underline{\mathbf{x}}_R = \mathbf{F}_2 \mathbf{P} \hat{\mathbf{s}}, \quad (8)$$

which is broadcast to all the  $K$  active destinations. Here,  $\mathbf{P} = \text{diag}\{\sqrt{p_1}, \dots, \sqrt{p_K}\}$  is the power allocation matrix used at the relay. The long-term average total transmit power constraint at the relay is thus given by

$$P_{\text{tx,R}} \triangleq \text{tr}(\underline{\mathbf{x}}_R \underline{\mathbf{x}}_R^H) \leq P_{R \max}, \quad (9)$$

where  $P_{\text{tx,R}}$  represents the average total transmit power at the relay, and  $P_{R \max}$  is the maximum average total transmit power available at the relay. The signal  $\mathbf{y}_D \in \mathbb{C}^{K \times 1}$  received at the  $K$  active destinations is given by

$$\mathbf{y}_D = \mathbf{G}_D \underline{\mathbf{x}}_R + \mathbf{n}_D = \mathbf{P} \hat{\mathbf{s}} + \tilde{\mathbf{G}}_D \underline{\mathbf{x}}_R + \mathbf{n}_D, \quad (10)$$

where  $\mathbf{n}_D \in \mathbb{C}^{K \times 1}$  denotes the AWGN at the destinations and it obeys  $\mathcal{CN}(\mathbf{0}, \sigma_D^2 \mathbf{I}_K)$ . Thus, the signal received at the  $k$ -th active destination is

$$\begin{aligned} y_{D,k} &= \sqrt{p_k} \mathbb{E}[\mathbf{g}_{D,k}^H \mathbf{f}_{2,k}] \hat{s}_k + \sqrt{p_k} (\mathbf{g}_{D,k}^H \mathbf{f}_{2,k} - \mathbb{E}[\mathbf{g}_{D,k}^H \mathbf{f}_{2,k}]) \hat{s}_k \\ &\quad + \sum_{j \neq k}^K \sqrt{p_j} \mathbf{g}_{D,k}^H \mathbf{f}_{2,j} \hat{s}_j + n_{D,k}, \end{aligned} \quad (11)$$

where  $n_{D,k}$  is the  $k$ -th element of  $\mathbf{n}_D$ , while  $\mathbf{f}_{2,k}$  is the  $k$ -th column of  $\mathbf{F}_2$ . The SINR at the destination  $U_{k+K}$  for the  $k$ -th transmitted data stream is given by [33]

$$\gamma_k^{(2)} = \frac{p_k \left| \mathbb{E}[\mathbf{g}_{D,k}^H \mathbf{f}_{2,k}] \right|^2}{p_k \text{Var}(\mathbf{g}_{D,k}^H \mathbf{f}_{2,k}) + \sum_{j \neq k}^K p_j \mathbb{E} \left[ \left| \mathbf{g}_{D,k}^H \mathbf{f}_{2,j} \right|^2 \right] + \sigma_D^2}. \quad (12)$$

As a result, the end-to-end achievable rate of the  $k$ -th mIoT device pair can be given by

$$\mathcal{R}_k = \min \left\{ \mathcal{R}_k^{(1)}, \mathcal{R}_k^{(2)} \right\}, \quad (13)$$

where  $\mathcal{R}_k^{(1)} = \log_2 \left( 1 + \gamma_k^{(1)} \right)$ ,  $\mathcal{R}_k^{(2)} = \log_2 \left( 1 + \gamma_k^{(2)} \right)$ .

An overhead occupying  $\tau_T = 2K$  symbol intervals is used to facilitate the pilot-based CE during each coherence interval of  $T$  symbols. Therefore, we have to take the overhead-induced dimensionality loss of  $2K/T$  into account when calculating the sum rate which is expressed as

$$\mathcal{R}_{\text{sum}} = \left( 1 - \frac{2K}{T} \right) \frac{B}{2} \sum_{k=1}^K \mathcal{R}_k. \quad (14)$$

### III. EE OPTIMIZATION PROBLEM FORMULATION

We employ a realistic power consumption model similar to those used in [24], [25], [34]. The total power consumption of the system considered is quantified as

$$P_{\text{tot}} = P_{\text{PA}} + P_{\text{C}}, \quad (15)$$

where we have

$$\begin{aligned} P_{\text{PA}} &= \frac{\eta_{\text{PA,d}}^{-1}}{2} \left( 1 - \frac{2K}{T} \right) K P_{\text{tx,d}} + \frac{\eta_{\text{PA,d}}^{-1} 4K^2}{T} \rho_r \sigma_r^2 \\ &\quad + \frac{\eta_{\text{PA,R}}^{-1}}{2} \left( 1 - \frac{2K}{T} \right) P_{\text{tx,R}}, \end{aligned} \quad (16)$$

$$P_{\text{C}} = P_{\text{FIX}} + P_{\text{TC}} + P_{\text{SIG}}, \quad (17)$$

with  $P_{\text{PA}}$  representing the power consumed by power amplifiers (PAs), in which  $P_{\text{tx,d}}$  and  $\rho_r \sigma_r^2$  are the data transmit power and pilot transmit power of each active source device, respectively, while  $\eta_{\text{PA,d}} \in (0, 1)$  and  $\eta_{\text{PA,R}} \in (0, 1)$  are the efficiency of the PAs at the devices and at the relay, respectively. Furthermore,  $P_{\text{C}}$  denotes the total circuit power consumption, in which  $P_{\text{FIX}}$  is a constant accounting for the fixed power consumption required for control signalling, site-cooling and the load-independent base-band signal processing,  $P_{\text{TC}}$  indicates the power consumption of the transceiver's radio-frequency (RF) chains, and  $P_{\text{SIG}}$  accounts for the power consumption of the load-dependent signal processing. To be more specific, we have

$$\begin{aligned} P_{\text{TC}} &= M P_{\text{R}} + 2K P_{\text{d}} + P_{\text{SYN}}, \\ P_{\text{SIG}} &= \frac{B}{T} \frac{8MK^2}{L_{\text{R}}} + B \left( 1 - \frac{2K}{T} \right) \frac{4MK}{L_{\text{R}}} \\ &\quad + \frac{B}{T} \frac{1}{3L_{\text{R}}} (K^3 + 9MK^2 + 3MK), \end{aligned} \quad (18)$$

where  $P_{\text{R}}$  and  $P_{\text{d}}$  represent the power required to run the circuit components attached to each antenna at the relay and at the devices, respectively, while  $P_{\text{SYN}}$  is the power consumed by the oscillator. The first term of  $P_{\text{SIG}}$  describes the power consumption of CE, while the remaining two terms account for the power required by the computation of the ZF detection matrix  $\mathbf{F}_1$  and the ZF precoding matrix  $\mathbf{F}_2$ . Still referring to (18),  $L_{\text{R}}$  denotes the computational efficiency quantified in terms of the complex-valued arithmetic operations per Joule at the relay. As a result, the EE  $\eta_{\text{EE}}$  [bits/Joule] is defined as<sup>3</sup>

$$\eta_{\text{EE}}(\mathbf{P}, \mathcal{S}, M) = \mathcal{R}_{\text{sum}} / P_{\text{tot}}. \quad (19)$$

It is plausible that  $\eta_{\text{EE}}$  is a function of the following system resources: the power allocation matrix  $\mathbf{P}$  used at the relay, the set  $\mathcal{S}$  of active mIoT device pairs, and the number of the relay antennas,  $M$ . In this paper, the energy-efficient resource allocation is formulated as the following optimization problem.

$$\begin{aligned} &\max_{\mathbf{P}, \mathcal{S}, M} \quad \eta_{\text{EE}}(\mathbf{P}, \mathcal{S}, M), \\ &\text{s.t.} \quad \text{C1: } P_{\text{tx,R}} \leq P_{R \max}, \\ &\quad \quad \text{C2: } \mathcal{S} \in \mathbb{U}, \\ &\quad \quad \text{C3: } M \in \{1, 2, \dots, M_{\max}\}, \\ &\quad \quad \text{C4: } p_k \geq 0, \quad k = 1, \dots, K, \\ &\quad \quad \text{C5: } \mathcal{R}_k \geq R_0, \quad k = 1, \dots, K, \end{aligned} \quad (20)$$

<sup>3</sup>It can be readily seen from (15)-(18) that the total power consumption highly depends on the number of relay antennas  $M$ , on the relay power allocation matrix  $\mathbf{P}$  and on the selection of the active mIoT device pairs  $\mathcal{S}$ . Choosing an appropriate power consumption model is of paramount importance, when dealing with the energy-efficient resource allocation in massive MIMO aided multi-pair relay mIoT.

where the objective function  $\eta_{\text{EE}}(\mathbf{P}, \mathcal{S}, M)$  is defined by (19). In (20), C1 ensures that the sum of power allocated to the  $K$  data streams does not exceed the maximum transmit power available to the relay, while C2 is a combinatorial constraint imposed on the device-pair selection, where  $\mathbb{U}$  denotes the group of all the available sets of active device pairs. The constraint associated with the number of relay antennas  $M$  is specified by C3, in which  $M_{\text{max}}$  is the largest possible number, and C4 is the boundary constraint of the relay power allocation variables. In addition, for some mIoT application scenarios (e.g., agriculture production detection), system energy is limited or electricity is generated by means of unpredictable renewable energy, such as wind and solar. One requirement in terms of the system operation is to guarantee appropriate QoS, which is a profile associated to each data instance. QoS can regulate the nonfunctional properties of information [35]. C5 represents the QoS constraint for each device pair, where  $\mathcal{R}_k$  is the achievable rate of the  $k$ -th pair device, and  $R_0$  is a given threshold.

#### IV. EE ANALYSIS OF THE MASSIVE MIMO AIDED MULTI-PAIR DF RELAY SYSTEM

From (14), (19) and (20), we can see that it is challenging to calculate the EE in real time, because the EE depends on specific LSF channel coefficients and requires challenging optimization involving matrix variables. To overcome this predicament, in this section, we firstly derive a closed-form expression of the EE under the assumption that the mIoT device locations are known. Subsequently, an EE expression is provided for the scenario where the device locations are assumed to be independent and uniformly distributed (i.u.d.) random variables in the coverage area. In these expressions, both the instantaneous channel coefficients and the matrix variables will disappear, hence the instantaneous CSI and the complex matrix calculations are no longer needed in our resource allocation.

##### A. EE Analysis Assuming Known Device Locations

In this subsection, upon assuming that the mIoT device locations are known *a priori* (i.e., the LSF channel coefficients are assumed to be perfectly estimated), we derive a closed-form expression of the EE. As the system rate  $\mathcal{R}_k$  for finite system dimensions is difficult to calculate, we consider the large system limit, where  $M$  and  $K$  grow infinitely large while keeping a finite ratio  $M/K$ . However, as we use the asymptotic analysis only as a tool provide tight approximations for finite  $M$ ,  $K$ . In what follows, we will derive deterministic approximations of the system rates  $\mathcal{R}_k$ . Thus, considering both the SE and total power consumption, a closed-form deterministic approximations of the EE in the system considered is presented in the following theorem.

**Theorem 1.** *Using linear ZF transceivers with imperfect CSI, as well as assuming that the mIoT device locations are known a priori, the EE of the massive MIMO aided multi-pair relay system considered can be calculated by*

$$\eta_{\text{EE}}(\mathbf{P}, \mathcal{S}, M) \xrightarrow{a.s.} \frac{\left(1 - \frac{2K}{T}\right) \frac{B}{2} \mathcal{R}(\mathbf{P}, \mathcal{S}, M)}{P_{\text{tot}}(\mathbf{P}, \mathcal{S}, M)}, \quad (21)$$

where

$$\mathcal{R}(\mathbf{P}, \mathcal{S}, M) = \sum_{k=1}^K \min \left\{ \mathcal{R}_k^{(1)}, \mathcal{R}_k^{(2)} \right\} \quad (22)$$

with  $\mathcal{R}_k^{(1)}$  and  $\mathcal{R}_k^{(2)}$  being calculated as

$$\begin{aligned} \mathcal{R}_k^{(1)} &\xrightarrow{a.s.} \log_2 \left( 1 + \frac{(M-K) P_{\text{tx},\mathbb{U}} \beta'_k}{P_{\text{tx},\text{d}} A_1 + \sigma_{\text{R}}^2} \right), \\ \mathcal{R}_k^{(2)} &\xrightarrow{a.s.} \log_2 \left( 1 + \frac{p_k}{\tilde{\beta}_{k+K} P_{\text{tx},\text{R}} + \sigma_{\text{D}}^2} \right), \end{aligned} \quad (23)$$

in which

$$A_1 = \sum_{j=1}^K (\beta_j - \beta'_j) = \sum_{j=1}^K \tilde{\beta}_j, \quad \tilde{\beta}_{k+K} = \beta_{k+K} - \beta'_{k+K}. \quad (24)$$

The total power consumption  $P_{\text{tot}}(\mathbf{P}, \mathcal{S}, M)$  is given by (15), where we have

$$P_{\text{tx},\text{R}} \xrightarrow{a.s.} \frac{\sum_{k=1}^K p_k (\beta'_{k+K})^{-1}}{M-K}. \quad (25)$$

*Proof:* See Appendix I. ■

According to (25), the long-term average total transmit power constraint (9) of the relay can be rewritten as

$$\frac{\sum_{k=1}^K p_k (\beta'_{k+K})^{-1}}{M-K} \leq P_{\text{R,max}}. \quad (26)$$

*Remark 1.* In Theorem 1, we obtain the closed-form expression of the EE, which only depends on the LSF channel coefficients of active mIoT device pairs and on the configurable system parameters. This expression is a fundamental one that characterizes the relationship between the EE and  $(\mathbf{P}, \mathcal{S}, M)$  for the general case, and acts as source in the subsequent section. In the expression, the complicated calculation involving large-dimensional matrix variables that represent the SSF channel coefficients is avoided.

In practical relay aided systems, the computational resources of the relay are limited. Hence, optimally solving the mixed-integer nonlinear optimization problem of (20) may become computationally unaffordable to the relay. As shown in Fig. 5, the average EE performance of the brute-force search aided optimal power allocation is only slightly higher than that of the equal power allocation strategy. Therefore, the equal power allocation strategy can be used at the relay for reducing the computational complexity of directly solving (20). More specifically, upon considering the equal power allocation that satisfies (26) for any  $k = 1, \dots, K$ , the power allocation coefficients are calculated as

$$p_k = \frac{(M-K) P_{\text{tx},\text{R}}}{A_2}, \quad \forall k, \quad (27)$$

where  $A_2 = \sum_{k=1}^K (\beta'_{k+K})^{-1}$ . As a result, compared to the optimal power allocation (21) that optimizes  $p_k$  ( $k = 1, \dots, K$ ) for each mIoT device pair, it becomes feasible for us to only optimize the total transmit power  $P_{\text{tx},\text{R}}$ , when the

relay's transmit power is equally allocated to all the destination devices.

Substituting (27) into (21), we arrive at the following corollary concerning the EE under the assumption of using equal power allocation at the relay.

**Corollary 1.** *The EE  $\bar{\eta}_{\text{EE}}$  associated with the equal power allocation at the relay is calculated as*

$$\bar{\eta}_{\text{EE}}(P_{\text{tx,R}}, \mathcal{S}, M) \xrightarrow{a.s.} \frac{(1 - \frac{2K}{T}) \frac{B}{2} \bar{\mathcal{R}}(P_{\text{tx,R}}, \mathcal{S}, M)}{P_{\text{tot}}(P_{\text{tx,R}}, \mathcal{S}, M)}, \quad (28)$$

where

$$\bar{\mathcal{R}}(P_{\text{tx,R}}, \mathcal{S}, M) = \sum_{k=1}^K \min \left\{ \bar{\mathcal{R}}_k^{(1)}, \bar{\mathcal{R}}_k^{(2)} \right\}, \quad (29)$$

with  $\bar{\mathcal{R}}_k^{(1)} = \mathcal{R}_k^{(1)}$  (given by (23)) and

$$\bar{\mathcal{R}}_k^{(2)} \xrightarrow{a.s.} \log_2 \left( 1 + \frac{(M-K) P_{\text{tx,R}}}{\left( \tilde{\beta}_{k+K} P_{\text{tx,R}} + \sigma_{\text{D}}^2 \right) A_2} \right). \quad (30)$$

Again,  $P_{\text{tot}}(P_{\text{tx,R}}, \mathcal{S}, M)$  is given by (15).

### B. EE Analysis Assuming i.u.d. Device Locations

In the previous subsection, we have derived the closed-form expression of the EE under the assumption that the device locations are known *a priori*. This assumption imposes an extremely high complexity burden and implementation cost, especially in high-mobility environments, because the channel coefficients will change rapidly and it is difficult to select the active device pairs instantly in practical mobile communication systems [36]. In this subsection, we consider a more general scenario in which the mMTC devices are assumed to be i.u.d. in the relay's coverage area, and derive the corresponding EE expression as a function of the total relay transmit power  $P_{\text{tx,R}}$ , the number of active mMTC device pairs  $|\mathcal{S}| = K$  and the number of relay antennas  $M$ . The EE expression obtained in this scenario provides further insights into the selection of EE-optimal system parameters.

We assume that the relay's coverage area is modelled as a disc and the relay is located at the geometric center of this disc. Furthermore, all the active source and destination devices are assumed to be i.u.d. in the disc, whose radius  $R$  satisfies  $R_{\text{min}} \leq R \leq R_{\text{max}}$ . The LSF channel coefficient of the  $k$ -th active mMTC device is modelled as  $\beta_k = c l_k^{-\alpha}$ , where  $l_k$  is the distance between the  $k$ -th mMTC device and the relay,  $\alpha$  is the path-loss exponent, and  $c$  is the path-loss at the reference distance  $R_{\text{min}}$ . The probability density function (PDF) of  $l_k$  is

$$f(l_k) = \frac{2l_k}{R_{\text{max}}^2 - R_{\text{min}}^2}, \quad R_{\text{min}} \leq l_k \leq R_{\text{max}}, \quad (31)$$

where  $R_{\text{max}}$  is the radius of the circular cell.

In Theorem 2, we first give the expression of the EE assuming i.u.d. device locations.

**Theorem 2.** *Given the other parameters, using linear ZF transceivers with imperfect SSF channel coefficients estimated by the MMSE estimator and assuming that all the devices*

*are i.u.d. in the relay's coverage area, the EE of the massive MIMO aided multi-pair relay system considered with equal relay power allocation is formulated as*

$$\tilde{\eta}_{\text{EE}}(P_{\text{tx,R}}, K, M) \xrightarrow{a.s.} \frac{(1 - \frac{2K}{T}) \frac{B}{2} \tilde{\mathcal{R}}(P_{\text{tx,R}}, K, M)}{P_{\text{tot}}(P_{\text{tx,R}}, K, M)}, \quad (32)$$

where

$$\tilde{\mathcal{R}}(P_{\text{tx,R}}, K, M) = K \min \left\{ \tilde{\mathcal{R}}_k^{(1)}, \tilde{\mathcal{R}}_k^{(2)} \right\}, \quad (33)$$

with

$$\tilde{\mathcal{R}}_k^{(1)} \xrightarrow{a.s.} \int_{R_{\text{min}}}^{R_{\text{max}}} \log_2 \left( 1 + \frac{(M-K) P_{\text{tx,U}} \beta_k'}{P_{\text{tx,d}} \tilde{A}_1 + \sigma_{\text{R}}^2} \right) f(l_k) dl_k, \quad (34)$$

$$\tilde{\mathcal{R}}_k^{(2)} \xrightarrow{a.s.} \int_{R_{\text{min}}}^{R_{\text{max}}} \log_2 \left( 1 + \frac{(M-K) P_{\text{tx,R}}}{\left( P_{\text{tx,R}} \tilde{\beta}_{k+K} + \sigma_{\text{D}}^2 \right) \tilde{A}_2} \right) \times f(l_{k+K}) dl_{k+K}, \quad (35)$$

$$\tilde{A}_1 = \frac{cK}{2K\rho_r (R_{\text{max}}^2 - R_{\text{min}}^2)} \left\{ R_{\text{max}}^2 {}_2F_1 \left( 1, \frac{1}{\alpha}; \frac{\alpha+2}{\alpha}; -\frac{R_{\text{max}}^\alpha}{2Kc\rho_r} \right) - R_{\text{min}}^2 {}_2F_1 \left( 1, \frac{1}{\alpha}; \frac{\alpha+2}{\alpha}; -\frac{R_{\text{min}}^\alpha}{2Kc\rho_r} \right) \right\}, \quad (36)$$

$$\tilde{A}_2 = \frac{K}{c(R_{\text{max}}^2 - R_{\text{min}}^2)} \left\{ \frac{1}{2K\rho_r} \frac{R_{\text{max}}^{2(\alpha+1)} - R_{\text{min}}^{2(\alpha+1)}}{c(\alpha+1)} + \frac{2(R_{\text{max}}^{\alpha+2} - R_{\text{min}}^{\alpha+2})}{\alpha+2} \right\}^2. \quad (37)$$

Again,  $P_{\text{tot}}(P_{\text{tx,R}}, K, M)$  is given by (15).

*Proof:* See Appendix II. ■

**Remark 2.** Theorem 2 characterizes the relationship between the EE and  $(P_{\text{tx,R}}, K, M)$  under the condition of equal power allocation and random device locations. According to Theorem 2, we are capable of evaluating the EE without using any channel coefficients and without complex matrix calculations. This results in a substantial complexity reduction of the real-time online computation. However, as far as solving the optimization problem associated with the energy-efficient resource allocation is concerned, (32) remains excessively complex due to the tedious integral in (33).

In order to circumvent the aforementioned obstacle, a lower bound of (32) is derived as follows.

**Corollary 2.** *A lower bound of (32) is given by*

$$\tilde{\eta}_{\text{EE}}(P_{\text{tx,R}}, K, M) \geq \tilde{\eta}_{\text{EELB}}(P_{\text{tx,R}}, K, M) = \frac{(1 - \frac{2K}{T}) \frac{BK}{2} \tilde{\mathcal{R}}_{\text{LB}}(P_{\text{tx,R}}, K, M)}{P_{\text{tot}}(P_{\text{tx,R}}, K, M)}, \quad (38)$$

where

$$\tilde{\mathcal{R}}_{\text{LB}}(P_{\text{tx,R}}, K, M) = \min \left\{ \tilde{\mathcal{R}}_{\text{LB}}^{(1)}, \tilde{\mathcal{R}}_{\text{LB}}^{(2)} \right\}, \quad (39)$$

with

$$\begin{aligned}\tilde{\mathcal{R}}_{\text{LB}}^{(1)} &= \log_2 \left( 1 + \frac{(M-K) K P_{\text{tx,d}}}{\left( P_{\text{tx,d}} \tilde{A}_1 + \sigma_{\text{R}}^2 \right) \tilde{A}_2} \right), \\ \tilde{\mathcal{R}}_{\text{LB}}^{(2)} &= \log_2 \left( 1 + \frac{(M-K) K P_{\text{tx,R}}}{\left( P_{\text{tx,R}} \tilde{A}_1 + K \sigma_{\text{D}}^2 \right) \tilde{A}_2} \right).\end{aligned}\quad (40)$$

*Proof:* See Appendix III. ■

*Remark 3.* It can be observed from Corollary 2 that the lower bound  $\tilde{\eta}_{\text{EELB}}(P_{\text{tx,R}}, M, K)$  and upper bound  $\tilde{\eta}_{\text{EEUB}}(P_{\text{tx,R}}, M, K)$  derived are represented by a simple closed-form expression without the tedious integral in (33), which is significantly beneficial for efficiently solving the optimization problem associated with our energy-efficient resource allocation.

## V. ENERGY-EFFICIENT RESOURCE ALLOCATION FOR MAXIMIZING THE LOWER BOUND OF THE EE

Let us commence with a brief discussion about the rationale and significance of the analytical results we have obtained so far. Theorem 1 quantifies the EE of the massive MIMO aided mIoT network considered under the assumption that the positions of the devices are known. The network considered in this paper is a narrow-band mIoT (NB-mIoT) network, which has been standardized in 3GPP Release 13 [37] to support a large number of low-power devices [38]. In addition, considering more general and practical mIoT application scenarios, e.g., environmental monitoring and agriculture inspection, where the devices are i.u.d. and their energy is limited, it is significantly vital for controlling electrical devices to properly address issues related to QoS and energy distribution. Theorem 2 gives the exact integral expression of the EE. However, it remains an open challenge to deal with an optimization problem whose objective function (i.e., the EE herein) is given by complex integrals. Traditional optimization tools, such as convex optimization, genetic algorithms, exhaustive search and so forth, become futile in this scenario. As a remedy, in Corollary 2, a simple lower bound of the EE is derived, where the tedious integral vanishes. Naturally, in this section, we reformulate the original energy-efficient resource allocation problem (20) as the following optimization problem<sup>4</sup> that maximizes the lower bound of the EE.

$$\begin{aligned}\max_{P_{\text{tx,R}}, K, M} \quad & \tilde{\eta}_{\text{EELB}}(P_{\text{tx,R}}, K, M), \\ \text{s.t.} \quad & \text{C1}' : M \in \{1, 2, \dots, M_{\text{max}}\}, \\ & \text{C2}' : K \in \{1, 2, \dots, M-1\}, \\ & \text{C3}' : 0 \leq P_{\text{tx,R}} \leq P_{\text{R,max}}, \\ & \text{C4}' : \tilde{\mathcal{R}}_{\text{LB}} \geq R_0.\end{aligned}\quad (41)$$

<sup>4</sup>This optimization problem is quite different from the conventional resource allocation problem that targets at specific mIoT device pairs. In this paper, we intend to optimize the EE, which is a system-level metric to be determined by solving the resource allocation optimization problem of (41). In particular, when solving (41), it is unnecessary for the relay to know the SSF and LSF components of the CSI of each mIoT device pair.

It is plausible that (41) is a non-convex problem, which remains mathematically challenging to solve. Nonetheless, it has become tractable. For obtaining the global optimal solution of (41), typically we have to carry out brute-force search over the feasible-solution space, which leads to a potentially prohibitive computational complexity. Therefore, instead of solving (41) directly, we propose a sub-optimal strategy by decomposing (41) into three subproblems, i.e., Subproblem I: optimization of the relay's transmit power  $P_{\text{tx,R}}$  for a given  $M, K$ ; Subproblem II: optimization of the number of relay antennas  $M$  for the given  $P_{\text{tx,R}}$  and  $K$ ; and Subproblem III: optimization of the number of active mIoT device pairs  $K$  for the given  $P_{\text{tx,R}}$  and  $M$ . Then, an iterative strategy is used, which solves this pair of subproblems sequentially in each iteration, as detailed below.

### A. Subproblem I: Optimization of the Relay's Transmit Power

For a given  $K$  and  $M$ , the subproblem of optimizing  $P_{\text{tx,R}}$  is written as

$$\begin{aligned}\max_{P_{\text{tx,R}}} \quad & \tilde{\eta}_{\text{EELB}}(P_{\text{tx,R}}), \\ \text{s.t.} \quad & \text{C3}', \text{C4}'\end{aligned}\quad (42)$$

which is a non-convex fractional programming problem due to the non-differentiable objective function  $\tilde{\eta}_{\text{EELB}}(P_{\text{tx,R}})$ . By introducing a slack variable  $\lambda$  ( $\lambda > 0$ ), (42) is transformed into a quasi-convex fractional programming problem as follows.

$$\begin{aligned}\max_{P_{\text{tx,R}}, \lambda} \quad & \tilde{\eta}_{\text{EELB}}(P_{\text{tx,R}}, \lambda) \\ \text{s.t.} \quad & \text{C3}', \lambda \geq R_0, \tilde{\mathcal{R}}_{\text{LB}}^{(1)} \geq \lambda, \tilde{\mathcal{R}}_{\text{LB}}^{(2)} \geq \lambda,\end{aligned}\quad (43)$$

where  $\tilde{\eta}_{\text{EELB}} = \frac{(1 - \frac{2K}{T}) \frac{BK}{2} \lambda}{P_{\text{CF}} + E_{\text{PA}} P_{\text{tx,R}}}$  with  $P_{\text{CF}} = \frac{\eta_{\text{PA,d}}^{-1}}{2} (1 - \frac{2K}{T}) K P_{\text{tx,d}} + \frac{4\eta_{\text{PA,d}}^{-1}}{T} K^2 \rho_{\text{r}} \sigma_{\text{R}}^2 + P_{\text{C}}$  and  $E_{\text{PA}} = \frac{\eta_{\text{PA,R}}^{-1}}{2} (1 - \frac{2K}{T})$ .

The objective of the optimization problem (43) is in a quasi-concave fractional form, which is difficult to address directly. Therefore, using Dinkelbach's algorithm [39], [40], we transform it into a parameterized subtractive form as follows.

$$\begin{aligned}F(\xi) \triangleq \max_{P_{\text{tx,R}}, \lambda} \quad & \left( 1 - \frac{2K}{T} \right) \frac{BK}{2} \lambda \\ & - \xi \left( P_{\text{CF}} + \frac{\eta_{\text{PA,R}}^{-1}}{2} \left( 1 - \frac{2K}{T} \right) P_{\text{tx,R}} \right) \\ \text{s.t.} \quad & \text{C3}', \lambda \geq R_0, \tilde{\mathcal{R}}_{\text{LB}}^{(1)} \geq \lambda, \tilde{\mathcal{R}}_{\text{LB}}^{(2)} \geq \lambda.\end{aligned}\quad (44)$$

In (44),  $F(\xi)$  is a strictly decreasing and continuous function, which is convex for all  $\xi \in \mathbb{R}$ . Moreover,  $F(\xi) = 0$  has a unique solution denoted by  $\xi^*$ . We know that  $F(\xi^*)$  and the objective function of (43) result in the same optimal solution, and the optimal objective function value of (43) is  $\xi^*$  [39], [40]. Therefore, the primal problem (43) is equivalent to the newly defined parametric problem (44). Let us now turn to solving the problem (44).

It is plausible that all the constraints of (44) are either affine or convex w.r.t  $(\lambda, P_{\text{tx,R}})$  for a given  $M, K$  and  $\xi$ . Similarly,

the objective function of (44) is also affine w.r.t  $(\lambda, P_{\text{tx,R}})$ . As a result, (44) is a concave optimization problem. It can be readily verified that (44) satisfies Slater's condition [41], hence the optimal solution of (44) may be obtained equivalently by solving its Lagrangian dual problem

$$\min_{\mu_1, \mu_2, \mu_3, \mu_4 \geq 0} \max_{P_{\text{tx,R}}, \lambda} \mathcal{L}(P_{\text{tx,R}}, \lambda, \mu_1, \mu_2, \mu_3, \mu_4), \quad (45)$$

where

$$\begin{aligned} \mathcal{L}(P_{\text{tx,R}}, \lambda, \mu_1, \mu_2, \mu_3, \mu_4) &= \left(1 - \frac{2K}{T}\right) \frac{BK}{2} \lambda \\ &- \xi \left( P_{\text{CF}} + \frac{\eta_{\text{PA,R}}^{-1}}{2} \left(1 - \frac{2K}{T}\right) \times P_{\text{tx,R}} \right) + \mu_1 \left( \tilde{\mathcal{R}}_{\text{LB}}^{(1)} - \lambda \right) \\ &+ \mu_2 \left( \tilde{\mathcal{R}}_{\text{LB}}^{(2)} - \lambda \right) + \mu_3 (P_{\text{Rmax}} - P_{\text{tx,R}}) + \mu_4 (\lambda - R_0), \end{aligned} \quad (46)$$

and  $\mu_1, \mu_2, \mu_3, \mu_4$  are the Lagrange multipliers.

The dual problem (45) can be decomposed into two layers: the inner-layer maximization problem and outer-layer minimization problem. The optimal solution of (45) may be readily obtained by an iterative method. To elaborate a little further, we first solve the following inner-layer maximization problem

$$\max_{P_{\text{tx,R}}, \lambda} \mathcal{L}(P_{\text{tx,R}}, \lambda, \mu_1, \mu_2, \mu_3, \mu_4) \quad (47)$$

for the fixed Lagrange multipliers  $\mu_1, \mu_2, \mu_3$  and  $\mu_4$ , as well as for the given parameters  $\xi, M, K$ . Let the first-order derivatives of  $\mathcal{L}$  w.r.t  $(\lambda, P_{\text{tx,R}})$  be zero, yielding

$$\begin{aligned} \frac{\partial \mathcal{L}}{\partial \lambda} &= \left(1 - \frac{2K}{T}\right) \frac{BK}{2} - \mu_1 - \mu_2 + \mu_4 = 0, \\ \frac{\partial \mathcal{L}}{\partial P_{\text{tx,R}}} &= \frac{\xi \eta_{\text{PA,R}}^{-1}}{2} \left( \frac{2K}{T} - 1 \right) - \mu_3 \\ &+ \frac{\mu_2}{\ln 2} \left( \frac{\alpha_1 + 1}{(\alpha_1 + 1) P_{\text{tx,R}} + \alpha_2} - \frac{1}{P_{\text{tx,R}} + \alpha_2} \right) = 0, \end{aligned} \quad (48)$$

where  $\alpha_1 = \frac{(M-K)K}{A_2 A_1}$  and  $\alpha_2 = \frac{K \sigma_{\text{D}}^2}{A_1}$ . The optimal transmit power  $P_{\text{tx,R}}^*$  is then calculated as

$$P_{\text{tx,R}}^* = \frac{- (\alpha_1 + 2) \alpha_2 + \sqrt{(\alpha_1 + 2)^2 \alpha_2^2 + 4 (\alpha_1 + 1) \alpha_3}}{2 (\alpha_1 + 1)}, \quad (49)$$

with  $\alpha_3 = \frac{\alpha_1 \alpha_2 \mu_2}{\left( \mu_3 + \frac{\xi \eta_{\text{PA,R}}^{-1}}{2} \left(1 - \frac{2K}{T}\right) \right) \ln 2}$  and

$$\mu_4 = \left( \frac{2K}{T} - 1 \right) \frac{BK}{2} + \mu_1 + \mu_2. \quad (50)$$

By substituting (50) into (46), (45) is rewritten as follows:

$$\min_{\mu_1, \mu_2, \mu_3 \geq 0} \max_{P_{\text{tx,R}}} \hat{\mathcal{L}}(P_{\text{tx,R}}, \mu_1, \mu_2, \mu_3), \quad (51)$$

where

$$\begin{aligned} \hat{\mathcal{L}}(P_{\text{tx,R}}, \mu_1, \mu_2, \mu_3) &= \left(1 - \frac{2K}{T}\right) \frac{BK}{2} R_0 \\ &- \xi \left( P_{\text{CF}} + \frac{\eta_{\text{PA,R}}^{-1}}{2} \left(1 - \frac{2K}{T}\right) P_{\text{tx,R}} \right) + \mu_1 \left( \tilde{\mathcal{R}}_{\text{LB}}^{(1)} - R_0 \right) \\ &+ \mu_2 \left( \tilde{\mathcal{R}}_{\text{LB}}^{(2)} - R_0 \right) + \mu_3 (P_{\text{Rmax}} - P_{\text{tx,R}}). \end{aligned} \quad (52)$$

For the outer-layer minimization problem, since the Lagrange function  $\hat{\mathcal{L}}$  is differentiable, the gradient method may be readily used for updating the Lagrange multipliers  $\mu_1, \mu_2$  and  $\mu_3$  as follows.

$$\begin{aligned} \mu_1^{(n+1)} &= \left[ \mu_1^{(n)} - \tau_{\mu_1} \left( \tilde{\mathcal{R}}_{\text{LB}}^{(1)} - R_0 \right) \right]^+, \\ \mu_2^{(n+1)} &= \left[ \mu_2^{(n)} - \tau_{\mu_2} \left( \tilde{\mathcal{R}}_{\text{LB}}^{(2)} (P_{\text{tx,R}}^*) - R_0 \right) \right]^+, \\ \mu_3^{(n+1)} &= \left[ \mu_3^{(n)} - \tau_{\mu_3} (P_{\text{Rmax}} - P_{\text{tx,R}}^*) \right]^+, \end{aligned} \quad (53)$$

where the superscript 'n' denotes the iteration index,  $\tau_{\mu_1}, \tau_{\mu_2}$  and  $\tau_{\mu_3}$  are the step sizes used for moving in the direction of the negative gradient for the dual variables  $\mu_1, \mu_2$  and  $\mu_3$ , respectively.

Finally, the optimization problem (43) under the given  $K$  and  $M$  can be solved by a two-stage iterative algorithm. In the first stage, the parameter  $\xi$  is updated using Dinkelbach's method [39], [40]. In the second stage, the optimal Lagrange multipliers and  $P_{\text{tx,R}}^*$  are obtained for the given  $\xi$ . The detailed iterative procedure is summarized in Algorithm 1.

---

**Algorithm 1** Iterative algorithm for optimizing the transmit power of the relay

---

- **Initialization:**  $\xi^{(0)} > 0, \mu_{10} > 0, \mu_{20} > 0, \mu_{30} > 0, \epsilon_1 > 0, \epsilon_2 > 0, \tau_{\mu_1}, \tau_{\mu_2}, \tau_{\mu_3}$  and  $m = 0$
  - **Repeat** (corresponding to the first stage)
    - $m \leftarrow m + 1, n = 0, \mu_1^{(0)} = \mu_{10}, \mu_2^{(0)} = \mu_{20}, \mu_3^{(0)} = \mu_{30}$ .
    - 1) **Repeat** (corresponding to the second stage)
      - 2)  $n \leftarrow n + 1$ .
      - 3) Calculate  $P_{\text{tx,R}}^*$  with (49) under the given  $\mu_1^{(n-1)}, \mu_2^{(n-1)}, \mu_3^{(n-1)}$  and  $\xi^{(m-1)}$ .
      - 4) Update  $\mu_1^{(n)}, \mu_2^{(n)}$  and  $\mu_3^{(n)}$  by (53).
      - 5)  $\Delta \mu_1 = \mu_1^{(n)} - \mu_1^{(n-1)}, \Delta \mu_2 = \mu_2^{(n)} - \mu_2^{(n-1)}, \Delta \mu_3 = \mu_3^{(n)} - \mu_3^{(n-1)}$ .
      - 6) **Until**  $|\Delta \mu_1| \leq \epsilon_1, |\Delta \mu_2| \leq \epsilon_1$  and  $|\Delta \mu_3| \leq \epsilon_1$ .
      - 7)  $\xi^{(m)} = \frac{(1 - \frac{2K}{T}) \frac{BK}{2} \tilde{\mathcal{R}}_{\text{LB}}(P_{\text{tx,R}}^*)}{P_{\text{CF}} + \frac{\eta_{\text{PA,R}}^{-1}}{2} (1 - \frac{2K}{T}) P_{\text{tx,R}}^*}$
  - **Until**
    - $\left| \left(1 - \frac{2K}{T}\right) \frac{BK}{2} \tilde{\mathcal{R}}_{\text{LB}}(P_{\text{tx,R}}^*) - \xi^{(m)} \right| \times \left( P_{\text{CF}} + \frac{\eta_{\text{PA,R}}^{-1}}{2} \left(1 - \frac{2K}{T}\right) P_{\text{tx,R}}^* \right) \leq \epsilon_2$
    - is satisfied.
    - $\xi^* \leftarrow \xi^{(m)}$ .
    - **Output**  $(\xi^*, P_{\text{tx,R}}^*)$ .
- 

*B. Subproblem II: Optimization of the Number of Relay Antennas*

Given  $P_{\text{tx,R}}$  and  $K$ , the optimization of the number of relay antennas is formulated as

$$\begin{aligned} \max_M \quad & \tilde{\eta}_{\text{EELB}}(M), \\ \text{s.t.} \quad & C1', C4'. \end{aligned} \quad (54)$$



We can observe that the optimization variable  $M$  in (54) takes integer value. Therefore, this optimization problem is an intractable non-convex problem. To address this challenge, we firstly relax  $M$  to a real variable  $M'$ . Then, by introducing a slack variable  $\chi$  ( $\chi > 0$ ), (54) is transformed into a quasi-convex fraction programming problem as follows.

$$\begin{aligned} & \max_{M', \chi} \widehat{\eta}_{\text{EELB}}(M', \chi), \\ & \text{s.t. } C1', \chi \geq R_0, \widetilde{\mathcal{R}}_{\text{LB}}^{(1)} \geq \chi, \widetilde{\mathcal{R}}_{\text{LB}}^{(2)} \geq \chi, \end{aligned} \quad (55)$$

where  $\widehat{\eta}_{\text{EELB}} = \frac{(1 - \frac{2K}{T}) \frac{BK}{2} \chi}{P_{\text{fixm}} + P_{\text{cm}} M'}$  with  $P_{\text{fixm}} = P_{\text{PA}} + P_{\text{FIX}} + P_{\text{PA}} + 2KP_{\text{U}} + P_{\text{SYN}} + \frac{B}{T} \frac{K^3}{3L_{\text{R}}}$  and  $P_{\text{cm}} = P_{\text{R}} + \frac{B}{T} \frac{8K^2}{L_{\text{R}}} + B(1 - \frac{2K}{T}) \frac{4K}{L_{\text{R}}} + \frac{B}{T} \frac{9K^2 + 3K}{3L_{\text{R}}}$ .

Compared to (43), it is easy to see that (55) has the completely exact same form as (43). Therefore, imitating Algorithm 1, we can obtain an optimal solution  $M'^*$  of (55). Finally, the optimal solution of  $M$  is calculated by  $M^* = \lceil M'^* \rceil$ , where  $\lceil \cdot \rceil$  is the ceiling function.

### C. Subproblem III: Optimization of the Number of Active Device Pairs

Given  $P_{\text{tx,R}}$  and  $M$ , the optimization of the number of active device pairs is formulated as

$$\begin{aligned} & \max_K \widetilde{\eta}_{\text{EELB}}(K), \\ & \text{s.t. } C2', C4'. \end{aligned} \quad (56)$$

Since the objective function of (56) involves the hypergeometric function, it is challenging to obtain the closed-form expression of the optimal solutions  $K^*$ . To elaborate a little further, we cannot relax  $K$  as a continuous variable  $K'$  for solving (56), since it is difficult to reformulate the hypergeometric function of (56) into a concave or quasi-concave function w.r.t.  $K'$ . Fortunately, the feasible region of (56) is  $\{1, 2, \dots, M-1\}$ , which is discrete and finite. Therefore, we can efficiently solve (56) using a one-dimensional search method.

So far, Subproblem I, Subproblem II and Subproblem III have been solved sequentially. In a similar fashion, the optimal solutions to the three subproblems are treated in turn as the initial values of each other in the remaining iterations, and the optimization problem (41) can then be efficiently solved relying on this iterative method. For the sake of clarity, our energy-efficient resource allocation algorithm conceived to maximize the lower bound of the EE is summarized as Algorithm 2.

## VI. CONVERGENCE AND COMPUTATIONAL COMPLEXITY ANALYSIS

In this section, we will present a convergence analysis of Algorithm 2 and a detailed complexity analysis so as to get a better insight into the computational complexity of the proposed algorithm.

From Section V, we know that Algorithm 2 includes three sequential solving processes corresponding to three subproblems. For Subproblem I, since (44) represents a convex

### Algorithm 2 Energy-efficient resource allocation algorithm for maximizing the lower bound of the EE

- **Input:** The maximum number of iterations  $N_{\text{loop}}$ , the accuracy tolerance  $\epsilon$ , and an initial value of the vector  $(P_{\text{tx,R}}, K, M)$
- **Output:**  $(P_{\text{tx,R}}^*, K^*, M^*)$

- 1) Assume  $n = 1$ ;
- 2) Update  $P_{\text{tx,R}}^{(n)}$  by Algorithm 1;
- 3) Replace  $M^{(n)}$  by the optimal solution obtained from solving (54) using the similar method updating  $P_{\text{tx,R}}^{(n)}$ ;
- 4) Replace  $K^{(n)}$  by the optimal solution obtained from solving (56) using the one-dimensional search method;
- 5)  $n \leftarrow n + 1$ , repeat 2), 3) and 4);
- 6) If

$$\begin{aligned} & \left| \widetilde{\eta}_{\text{EELB}}(P_{\text{tx,R}}^{(n)}, K^{(n)}, M^{(n)}) - \widetilde{\eta}_{\text{EELB}} \right. \\ & \quad \left. \times (P_{\text{tx,R}}^{(n-1)}, K^{(n-1)}, M^{(n-1)}) \right| < \epsilon \end{aligned}$$

or  $n = N_{\text{loop}}$ ,

then stop the iteration;

- 7)  $(P_{\text{tx,R}}^*, K^*, M^*) \leftarrow (P_{\text{tx,R}}^{(n)}, K^{(n)}, M^{(n)})$ .

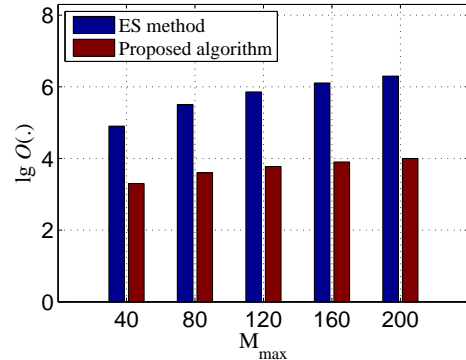


Fig. 3: Complexity comparisons of Algorithm 2 and the ES method against different  $M_{\text{max}}$ s. Note that the y-axis uses a base 10 logarithmic scale.

optimization problem w.r.t.  $(\lambda, P_{\text{tx,R}})$ , it is guaranteed that the solutions obtained in the second stage of Algorithm 1 converge to the optimal solution  $P_{\text{tx,R}}^*$  for each given  $\xi$ . Moreover, according to [41], the first stage of Algorithm 1 is also guaranteed to converge, since it sequentially looks for the optimal value of the univariate parameter  $\xi^*$  with the aid of multiple iterations. Therefore, subproblem I can converge to a unique value. For Subproblem II, since it has the same solving process as Subproblem I, Subproblem II can also converge to a fixed value and obtain an optimal solution of  $M$ . As for Subproblem III, the optimal solution of  $K$  is obtained by exhaustive search (ES). As a result, the proposed Algorithm 2 eventually converges. In Section VII, we have carried out extensive numerical simulations, where the convergence of Algorithm 2 is always empirically achieved.

From (20), we can see that  $\eta_{\text{EE}}$  in the original optimization problem is a function of the relay power allocation matrix,

$\mathbf{P}$ , the set of active mMTC device pairs,  $\mathcal{S}$ , and the number of the relay antennas,  $M$ . This is a complicated non-convex problem, so we can only employ the ES method to find its optimal solution. Because  $\mathbf{P} = \text{diag}\{\sqrt{p_1}, \dots, \sqrt{p_K}\}$ , the optimal solution of  $\mathbf{P}$  can be found by searching over  $p_1, p_2, \dots, p_K$  under the assumption that each of them takes discrete values [42]. Thus, the computational complexity of this step is  $O(D^K)$ , where  $D$  is the number of power levels that can be taken by  $p_k$ . Since there are  $K$  pairs of active mMTC devices in the set,  $\mathcal{S}$ , and all of them are selected from the group of all the available sets of active UE pairs ( $K \leq M - 1$ ), the complexity of UE-pair selection is  $O(C_{M-1}^K)$ . Furthermore,  $M$  is a discrete and finite variable. As a result, the total complexity of solving (20) by using the ES method is  $O(\sum_{M=1}^{M_{\max}} \sum_{K=1}^{M-1} M C_{M-1}^K D^K) = O([M_{\max} D (2(D+1)^{M_{\max}} - M_{\max} D - D) - 2(D+1)^{M_{\max}+2}] / (2D^2))$ . As the largest number of the relay antennas  $M_{\max}$  is large enough, the computational complexity is approximately equal to  $O(M_{\max} D^{M_{\max}-1})$ .

The reformulated optimization problem (41) is also a non-convex problem. To obtain the global optimal solution of (41), we have to use the ES method over the feasible-solution space. Thus, the total complexity is  $O(D' M_{\max} (M_{\max} - 1))$ , where  $D'$  denotes the number of power level of relay's total transmit power,  $P_{\text{tx,R}}$ . When  $M_{\max}$  is large enough, the computational complexity is approximately equal to  $O(D' M_{\max}^2)$ . Compared with the computational complexity of solving (20), it is obvious that the computational complexity of solving (41) has been significantly reduced.

On the other hand, since the ES method can lead to a prohibitive computational complexity, we propose Algorithm 2 to solve (41) by decomposing this problem into three subproblems. Assume that  $I_{\text{in1}}$  is the number of inner iterations required for reaching convergence of  $\xi$  by using the Dinkelbach's method in subproblem I. The complexity of updating the relay's total transmit power  $P_{\text{tx,R}}$  is  $O(3I_{\text{in1}}I_{\text{ou1}})$ , where  $I_{\text{ou1}}$  is the number of outer iterations. Similarly, in subproblem II, the complexity of updating the number of relay antennas  $M$  is  $O(3I_{\text{in2}}I_{\text{ou2}})$ , where  $I_{\text{in2}}$  and  $I_{\text{ou2}}$  are the number of inner and outer iterations in subproblem II, respectively. The one-dimensional search method used in subproblem III has a complexity of  $O(M_{\max} - 1)$ . If Algorithm 2 converges after  $I_{\text{loop}}$  iterations, the total complexity is  $O(I_{\text{loop}}(3I_{\text{in1}}I_{\text{ou1}} + 3I_{\text{in2}}I_{\text{ou2}} + M_{\max} - 1))$ . When  $M_{\max}$  is large enough, the computational complexity is approximately equal to  $O(I_{\text{loop}}M_{\max})$ . We can see that the computational complexity of the proposed algorithm is greatly less than that of the ES method when  $D'$  is comparable to  $I_{\text{loop}}$ . In Fig. 3, we compare the computational complexity of the proposed algorithm with that of the ES method in terms of the largest number of the relay antennas  $M_{\max}$ , where  $D' = 50$  and  $I_{\text{loop}} = 50$ . It is observed that Algorithm 2 exhibits a complexity reduction significantly compared with the ES method for any  $M_{\max}$ .

## VII. NUMERICAL RESULTS

In this section, we evaluate the EE performance of the massive MIMO aided mMTC network and demonstrate the

accuracy of our analytical results via numerical simulations. As a strong candidate for supporting mMTC communications [43], a small-cell cellular network is considered, and the simulation parameters are summarized in Table I. All the simulation parameters in this table are in accordance with the narrow-band IoT (NB-IoT) network [37] which promises to improve the cellular systems for mMTC by supporting a large number of IoT devices [38]. As part of 3GPP Release 13 [37], NB-IoT has been standardized for mMTC, and the required bandwidth for NB-IoT is 180 KHz for both uplink and downlink. Our numerical studies will demonstrate the efficiency of the proposed optimization strategy, and the impact of several relevant system parameters on the optimal relay transmit power, on the optimal number of relay antennas and on the optimal selection of the active mMTC device pairs.

Table I: Simulation Parameters

| Parameter  | Value                     |
|--|---------------------------|
| Reference distance: $R_{\min}$                   | 35 m                      |
| LSF model: $\beta_k = cl_k^{-\alpha}$            | $10^{-0.53} / l_k^{3.76}$ |
| Transmission bandwidth: $B$                      | 20 MHz                    |
| Channel coherence bandwidth: $B_c$               | 180 KHz                   |
| Channel coherence time: $T_c$                    | 10 ms                     |
| Fixed power consumption: $P_{\text{FIX}}$        | 18 W                      |
| Total noise power: $B\sigma^2$                   | -96 dBm                   |
| Computational efficiency at the relay: $L_R$     | 12.8 Gflops/W             |
| PA efficiency at the relay: $\eta_{\text{PA,R}}$ | 0.39                      |
| PA efficiency at devices: $\eta_{\text{PA,U}}$   | 0.3                       |
| Circuit power consumption at the relay: $P_R$    | 1 W                       |
| Circuit power consumption at devices: $P_d$      | 0.1 W                     |

### A. Accuracy of the Analytical EE

In Fig. ??, the EE  $\eta_{\text{EE}}$  and the corresponding average rate defined as  $\mathcal{R} = \frac{1}{K} \sum_{k=1}^K \mathcal{R}_k$  are numerically evaluated assuming  $R_{\max} = 250$  m,  $R_0 = 1$  bit/s/Hz, and  $P_{\text{tx,d}} = 20$  dBm. We also show the analytical EE given in (28) and the corresponding average rate derived from (29) (marked as Appx. 1), the analytical EE given in (32) and the corresponding average rate derived from (33) (marked as Appx. 2), as well as the EE lower bound given in (38) and the corresponding rate (39) (marked as LB). Moreover, when device locations have non-uniform distribution, simulation values of the EE (marked as Sim.) are also provided. To construct a non-uniform distribution across the whole coverage area, we segment the coverage area into two nested circular cells, where active mMTC devices of the two cells follow uniform distributions with different probability densities. The radii of the nested circular cells are 100 m and 250 m, respectively. It can be clearly seen from Fig. ?? that the analytical EE expressions derived and the EE lower bound are accurate even in a system of finite dimensions. Moreover, Fig. ??(a)-Fig. ??(c) show the EE versus the number of active mMTC device pairs,  $K$ , versus the number of relay antennas  $M$ , and versus the relay's transmit power  $P_{\text{tx,R}}$ , respectively. Meanwhile, the corresponding average rate is shown in Fig. ??(d)-Fig. ??(f). It can be observed from Fig. ??(a)-Fig. ??(c) that given the values of the other parameters, regardless of whether the quality of CE is high (e.g., when  $\rho_r = 100$ , as shown by the purple curves) or not (e.g., when  $\rho_r = 0.1$ ,

as shown by the blue curves), the EE is not a monotonically increasing/decreasing function of  $K$ ,  $M$  or  $P_{\text{tx,R}}$ . The optimal value of  $K$ ,  $M$  or  $P_{\text{tx,R}}$  maximizing the EE is usually not on the boundary. However, the average rate increases with  $M$  and  $P_{\text{tx,R}}$ , but decreases with  $K$ . Explicitly, in order to improve the average rate of all the active device pairs, the system needs more relay antennas, higher relay transmit power, or fewer pairs of active mIoT devices supported simultaneously. Furthermore, as shown in Fig. ??(a)-Fig. ??(c), it is worth noting that the lower bound given by (38) is close to the analytical EE of (32). Therefore, (38) is a sufficiently tight lower bound. At the same time, when the assumption that all the devices follow i.u.d. does not hold, the EE performance will degrade owing to model mismatch.

### B. Convergence and Optimality of the Proposed Optimization Strategy

In Fig. 5, we show the convergence of the proposed iterative resource allocation approach presented in Algorithm 2 by examining the EE attained versus the number of iterations. It can be observed that the maximum EE obtained using Algorithm 2 appears after 8 iterations, and this maximum EE value is indeed generated by the optimum system parameters of  $(P_{\text{tx,R}}^*, K^*, M^*) = (36.6, 31, 81)$ . In order to show the optimality of Algorithm 2, we provide a pair of performance benchmarks that correspond to solving the problem (20) based on *Theorem 1* (i.e., using optimal power allocation) and on *Theorem 2* (i.e., using equal power allocation) via the high-complexity brute-force searching (i.e., exhaustive searching), respectively. It is observed that after Algorithm 2 converges, the gap between the EE values achieved by Algorithm 2 and by solving the problem (20) based on *Theorem 2* with the brute-force searching becomes small. Moreover, the optimum system parameters obtained by solving (20) based on *Theorem 2* using the brute-force searching are  $(P_{\text{tx,R}}^*, K^*, M^*) = (37, 30, 81)$ , which are also close to those achieved by Algorithm 2. Therefore, the proposed Algorithm 2 is near-optimal. It represents an appealing design option, because it is capable of substantially reducing the computational complexity at the expense of a marginal performance loss. Meanwhile, the gap between the two benchmarking algorithms is also small, which justifies the employment of the low-complexity equal power allocation at the relay.

In Fig. 6(a)-Fig. 6(c), we investigate the impact of the coverage area radius  $R_{\text{max}}$  on the optimum system parameters  $P_{\text{tx,R}}^*$ ,  $\rho_{\text{UE}}^*$ , and  $M^*$ , respectively, where  $\rho_{\text{UE}} = \frac{K}{\pi(R_{\text{max}}^2 - R_{\text{min}}^2)}$  is the density of the active mIoT device pairs in the given relay's coverage area. The corresponding optimum EE is shown in Fig. 6(d). We can readily observe that as  $R_{\text{max}}$  becomes large,  $P_{\text{tx,R}}^*$  and  $M^*$  are increased, while  $\rho_{\text{UE}}^*$  is decreased. In other words, for the sake of optimizing the EE, the optimum design should increase the relay's transmit power, use more antennas at the relay and reduce the device density, if a larger coverage area of the relay is required. This conclusion is also supported by the results shown in Fig. 6(d), where we can see that the optimum EE is indeed reduced when the coverage area of the relay becomes larger, provided that

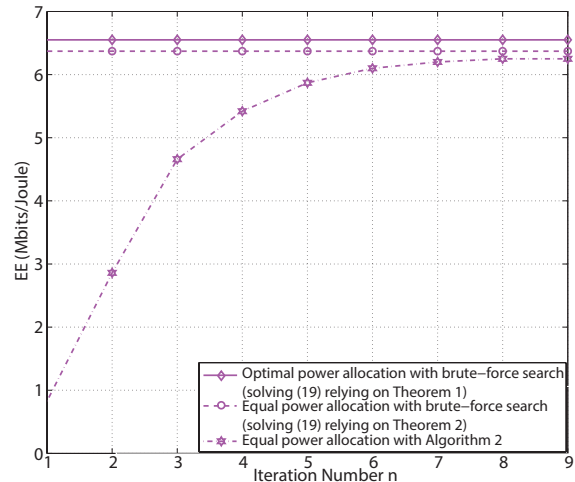


Fig. 5: Convergence and optimality of the proposed Algorithm 2. Assume  $R_0 = 1$  bit/s/Hz,  $M_{\text{max}} = 128$ ,  $P_{\text{R,max}} = 50$  dBm,  $\rho_r = 100$ , and  $P_{\text{tx,U}} = 20$  dBm.

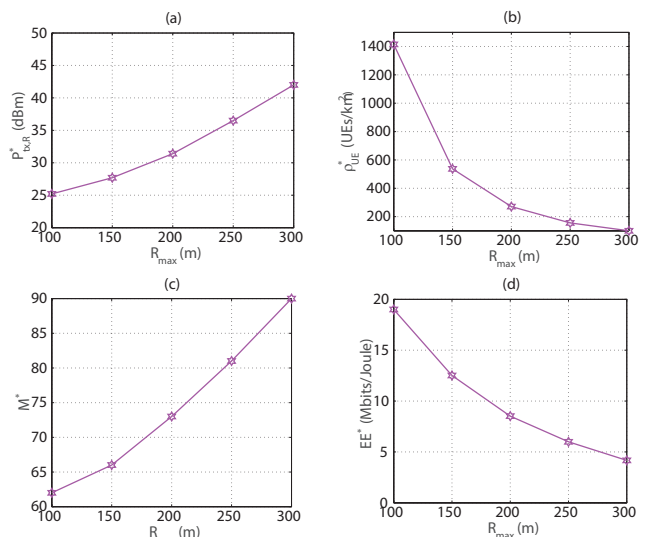


Fig. 6: The optimum EE and the optimum system parameters  $(P_{\text{tx,R}}^*, \rho_{\text{UE}}^*, M^*)$  versus different values of  $R_{\text{max}}$ . Assume  $\rho_r = 100$ ,  $R_0 = 1$  bit/s/Hz,  $M_{\text{max}} = 128$ ,  $P_{\text{R,max}} = 50$  dBm, and  $P_{\text{tx,d}} = 20$  dBm.

the values of the other system parameters remain unchanged. In fact, it is readily seen that we will have  $\eta_{\text{EE}}^* \rightarrow 0$  as  $R_{\text{max}} \rightarrow +\infty$ .

In Fig. 7(a)-Fig. 7(c), we show the impact of the CE quality indicator  $\rho_r$  on the optimum system parameters  $(P_{\text{tx,R}}^*, \rho_{\text{UE}}^*, M^*)$ . We can observe from these figures that in poor CE scenarios, a higher relay transmit power, more active devices and more relay antennas should be used to make the system energy-efficient. Moreover, as expected, it can be readily observed from Fig. 7(d) that high-quality CE is capable of providing a high EE. Additionally, as  $\rho_r$  becomes large, the increase of the EE slows down and converges to the value that relies on perfect CSI estimation. This implies that although the system associated with high-quality CE (i.e.

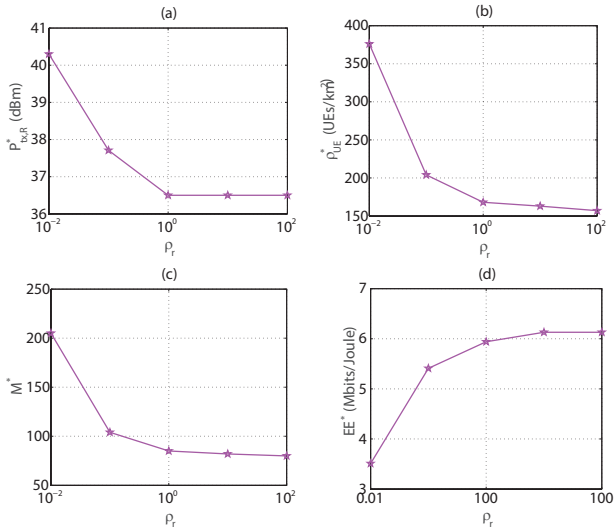


Fig. 7: The optimum EE and the optimum system parameters ( $P_{\text{tx,R}}^*$ ,  $\rho_{\text{UE}}^*$ ,  $M^*$ ) versus the CE quality indicator  $\rho_r$ . Assume  $R_{\text{max}} = 250$  m,  $R_0 = 1$  bit/s/Hz,  $M_{\text{max}} = 128$ ,  $P_{\text{Rmax}} = 50$  dBm, and  $P_{\text{tx,d}} = 20$  dBm.

$\rho_r = 10^2$ ) is capable of achieving a better EE performance than the system with poor CE (i.e.  $\rho_r = 10^{-1}$ ), the pursuit of extremely high CE accuracy is unnecessary (e.g.,  $\rho_r \geq 1$  is shown to be adequate by our simulations).

In Fig. 8(a)-Fig. 8(d), we show the optimum system parameters ( $P_{\text{tx,R}}^*$ ,  $\rho_{\text{UE}}^*$ ,  $M^*$ ) and the corresponding optimum EE versus the variations of the QoS constraint  $R_0$ , respectively. It can be observed that for  $R_0 \leq 4$  bit/s/Hz, the value of ( $P_{\text{tx,R}}^*$ ,  $\rho_{\text{UE}}^*$ ,  $M^*$ ) remains unchanged, but for  $R_0 > 4$  bit/s/Hz, ( $P_{\text{tx,R}}^*$ ,  $\rho_{\text{UE}}^*$ ,  $M^*$ ) increases with the increase of  $R_0$ . To be more specific, in our simulations, the optimum system parameters obtained using Algorithm 2 under the assumption of  $R_0 \leq 4$  bit/s/Hz is ( $P_{\text{tx,R}}^*$ ,  $\rho_{\text{UE}}^*$ ,  $M^*$ ) = (36.4, 155.8, 81), which results in a QoS constraint of  $\tilde{R}_{\text{LB}} = 5.53$  bit/s/Hz. Therefore, in the case of  $R_0 \geq 5.53$  bit/s/Hz, the optimal solution is found along the edges of the feasible region that is affected by the QoS constraint.

### VIII. CONCLUSION

We have provided a series of analytical EE expressions for the mIoT network using a massive MIMO aided multi-pair DF relay, and proposed an iterative optimization strategy to maximize the lower bound of the EE. Firstly, upon assuming that the mIoT device locations are known *a priori*, a closed-form expression of the EE was derived. The expression obtained only depends on the LSF channel coefficients and the configurable system parameters. Secondly, an exact integral expression of the EE was derived for a more general scenario, where each device's position is assumed to be an i.u.d random variable in the relay's coverage area. Moreover, in order to bypass solving complex integrals, we derived a simple but efficient lower bound of the EE. Finally, a low-complexity iterative resource allocation strategy was proposed to maximize this lower bound. Our numerical results demonstrated the

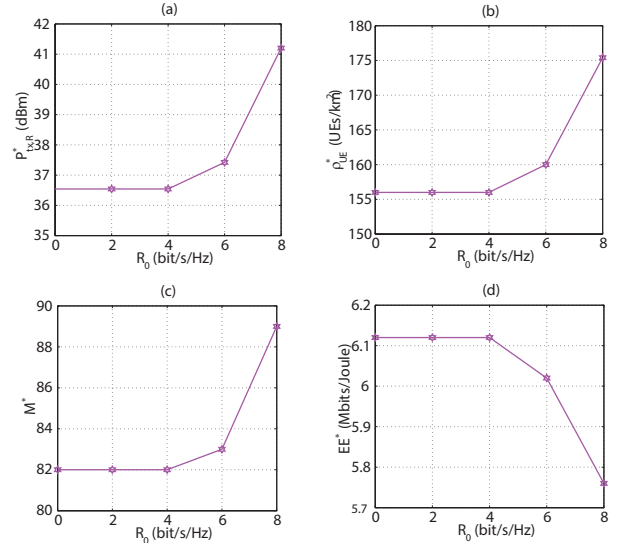


Fig. 8: The optimum EE and the optimum system parameters ( $P_{\text{tx,R}}^*$ ,  $\rho_{\text{UE}}^*$ ,  $M^*$ ) versus the QoS constraint  $R_0$ , assuming  $R_{\text{max}} = 250$  m,  $\rho_r = 100$ ,  $M_{\text{max}} = 128$ ,  $P_{\text{Rmax}} = 50$  dBm, and  $P_{\text{tx,d}} = 20$  dBm.

accuracy of the analytical expressions derived, and verified the effectiveness and convergence speed of the proposed strategy. For future work, it would be interesting to study the energy-efficient problems in mobile IoT environments instead of the assumption that the locations of all the devices are fixed in this paper. We will also derive an exact integral-based expression of the EE under the assumption that the locations of devices are non-uniform distribution.

### APPENDIX I PROOF OF THEOREM 1

Firstly,  $\gamma_k^{(1)}$  is derived. Observing (7), we have to calculate  $\mathbb{E}[\mathbf{f}_{1,k}^H \mathbf{g}_{\text{S},k}]$ ,  $\text{Var}(\mathbf{f}_{1,k}^H \mathbf{g}_{\text{S},k})$ ,  $\mathbb{E}[\|\mathbf{f}_{1,k}\|^2]$  and  $\sum_{j \neq k}^K \mathbb{E}[\|\mathbf{f}_{1,k}^H \mathbf{g}_{\text{S},j}\|^2]$ . Since  $\mathbf{F}_1 = (\hat{\mathbf{G}}_{\text{S}}^H \hat{\mathbf{G}}_{\text{S}})^{-1} \hat{\mathbf{G}}_{\text{S}}^H$ , we have

$$\mathbf{F}_1 \hat{\mathbf{G}}_{\text{S}} = \mathbf{F}_1 (\hat{\mathbf{G}}_{\text{S}} + \tilde{\mathbf{G}}_{\text{S}}) = \mathbf{I}_K + \mathbf{F}_1 \tilde{\mathbf{G}}_{\text{S}}, \quad (57)$$

which leads to

$$\mathbb{E}[\mathbf{f}_{1,k}^H \mathbf{g}_{\text{S},k}] = 1, \text{Var}[\mathbf{f}_{1,k}^H \mathbf{g}_{\text{S},k}] = \mathbb{E}[\|\mathbf{f}_{1,k} \tilde{\mathbf{g}}_{\text{S},k}\|^2]. \quad (58)$$

Then, we calculate  $\mathbb{E}[\|\mathbf{f}_{1,k}\|^2]$  and  $\text{Var}[\mathbf{f}_{1,k}^H \mathbf{g}_{\text{S},k}]$ . Applying [44, Theorem 14.3], we can obtain

$$\|\mathbf{f}_{1,k}\|^2 \xrightarrow{a.s.} \frac{\psi}{\frac{M}{K}\phi^2 - \psi} \frac{1}{K} \beta_k'^{-1}, \quad (59)$$

where  $\phi$  and  $\psi$  are the unique solutions of

$$\begin{aligned} \phi &= \frac{1}{M} \text{tr} \left( \mathbf{I}_M + \frac{K}{M} \frac{1}{\phi} \mathbf{I}_M \right)^{-1}, \\ \psi &= \frac{1}{M} \text{tr} \left( \mathbf{I}_M + \frac{K}{M} \frac{1}{\phi} \mathbf{I}_M \right)^{-2}. \end{aligned} \quad (60)$$

By solving the equation set (??), we can get  $\phi$  and  $\psi$ . Thus, for (59), we have

$$\|\mathbf{f}_{1,k}\|^2 \xrightarrow{a.s.} \frac{\beta'_k{}^{-1}}{M-K}. \quad (61)$$

By the dominated convergence theorem [45] and the continuous mapping theorem [46], it is straightforward to show that

$$\mathbb{E} \left[ \|\mathbf{f}_{1,k}\|^2 \right] - \frac{\beta'_k{}^{-1}}{M-K} \xrightarrow{a.s.} 0. \quad (62)$$

Furthermore, since  $\mathbf{f}_{1,k}$  and  $\tilde{\mathbf{g}}_{S,k}$  are independent, we have

$$\begin{aligned} \text{Var} [\mathbf{f}_{1,k}^H \mathbf{g}_{S,k}] &= \mathbb{E} \left[ |\mathbf{f}_{1,k}^H \tilde{\mathbf{g}}_{S,k}|^2 \right] = (\beta_k - \beta'_k) \mathbb{E} \left[ \|\mathbf{f}_{1,k}\|^2 \right] \\ &\xrightarrow{a.s.} \frac{(\beta_k - \beta'_k) \beta'_k{}^{-1}}{M-K}. \end{aligned} \quad (63)$$

Next, we calculate  $\sum_{j \neq k}^K \mathbb{E} \left[ |\mathbf{f}_{1,k}^H \tilde{\mathbf{g}}_{S,j}|^2 \right]$ . From (57), we see that  $\mathbf{f}_{1,k}^H \mathbf{g}_{S,j} = \mathbf{f}_{1,k}^H \tilde{\mathbf{g}}_{S,j}$  for  $j \neq k$ . Thus, we have

$$\begin{aligned} \mathbb{E} \left[ |\mathbf{f}_{1,k}^H \mathbf{g}_{S,j}|^2 \right] &= \mathbb{E} \left[ |\mathbf{f}_{1,k}^H \tilde{\mathbf{g}}_{S,j}|^2 \right] = (\beta_j - \beta'_j) \mathbb{E} \left[ \|\mathbf{f}_{1,k}\|^2 \right] \\ &\xrightarrow{a.s.} \frac{(\beta_j - \beta'_j) \beta'_k{}^{-1}}{M-K}. \end{aligned} \quad (64)$$

Naturally, we can obtain

$$\sum_{j \neq k}^K \mathbb{E} \left[ |\mathbf{f}_{1,k}^H \tilde{\mathbf{g}}_{S,i}|^2 \right] \xrightarrow{a.s.} \frac{\beta'_k{}^{-1} \sum_{j \neq k}^K (\beta_j - \beta'_j)}{M-K}. \quad (65)$$

Substituting (58), (62), (63) and (65) into (7), we have

$$\gamma_k^{(1)} \xrightarrow{a.s.} \frac{P_{\text{tx,U}} (M-K) \beta'_k}{P_{\text{tx,U}} \sum_{i=1}^K (\beta_i - \beta'_i) + \sigma_{\text{R}}^2}. \quad (66)$$

Secondly,  $P_{\text{tx,R}}$  is derived. According to (8) and (9), we have

$$\begin{aligned} P_{\text{tx,R}} &\triangleq \text{tr} (\mathbf{X}_{\text{R}} \mathbf{X}_{\text{R}}^H) = \text{tr} (\mathbf{F}_2 \mathbf{P} \hat{\mathbf{S}} \hat{\mathbf{S}}^H \mathbf{P}^H \mathbf{F}_2^H) \\ &= \text{tr} \left( \mathbf{P}^2 \left( \hat{\mathbf{G}}_{\text{D}}^H \hat{\mathbf{G}}_{\text{D}} \right)^{-1} \right) = \sum_{k=1}^K p_k \|\mathbf{f}_{2,k}\|^2 \\ &\xrightarrow{a.s.} \frac{\sum_{k=1}^K p_k \beta'_{k+K}{}^{-1}}{M-K}. \end{aligned} \quad (67)$$

Thirdly,  $\gamma_k^{(2)}$  is derived. Observing (12), we need to calculate  $\mathbb{E} \left[ \mathbf{g}_{\text{D},k}^H \mathbf{f}_{2,k} \right]$ ,  $\text{Var} \left( \mathbf{g}_{\text{D},k}^H \mathbf{f}_{2,k} \right)$  and  $\mathbb{E} \left[ |\mathbf{g}_{\text{D},k}^H \mathbf{f}_{2,j}|^2 \right]$ . Following the same methodology used for calculating  $\gamma_k^{(1)}$ , we have

$$\begin{aligned} \mathcal{E} \left[ \mathbf{g}_{\text{D},k}^H \mathbf{f}_{2,k} \right] &\xrightarrow{a.s.} 1, \\ \text{Var} \left( \mathbf{g}_{\text{D},k}^H \mathbf{f}_{2,k} \right) &\xrightarrow{a.s.} \frac{(\beta_{k+K} - \beta'_{k+K}) \beta'_{k+K}{}^{-1}}{M-K}, \\ \sum_{j \neq k}^K p_j \mathbb{E} \left[ |\mathbf{g}_{\text{D},k}^H \mathbf{f}_{2,j}|^2 \right] &\xrightarrow{a.s.} \frac{(\beta_{k+K} - \beta'_{k+K}) \sum_{j \neq k}^K p_j \beta'_{k+K}{}^{-1}}{M-K}. \end{aligned} \quad (68)$$

Substituting (67) and (68) into (12), we obtain

$$\gamma_k^{(2)} \xrightarrow{a.s.} \frac{p_k}{P_{\text{tx,R}} (\beta_{k+K} - \beta'_{k+K}) + \sigma_{\text{D}}^2}. \quad (69)$$

Finally, according to (13) and (19), we prove that (21) holds.  $\square$

## APPENDIX II PROOF OF THEOREM 2

According to the assumption that all the mMOT devices are i.i.d., and the strong law of large numbers, the value of  $A_1$  converges *almost surely* to its expected value when  $K$  is sufficiently large, i.e., we have  $A_1 \xrightarrow{a.s.} \tilde{A}_1$  when  $K \rightarrow \infty$ . This condition can be easily satisfied in massive MIMO systems. As a result,  $\tilde{A}_1$  is calculated as

$$\begin{aligned} A_1 &\xrightarrow{a.s.} \tilde{A}_1 = K \mathbb{E}_{l_k} \left[ \tilde{\beta}_k \right] = Kc \int_{R_{\min}}^{R_{\max}} \frac{1}{l_k^\alpha + 2cK\rho_{\text{r}}} f(l_k) dl_k \\ &= \frac{cK}{2K\rho_{\text{r}} (R_{\max}^2 - R_{\min}^2)} \left\{ R_{\max}^2 {}_2F_1 \left( 1, \frac{1}{\alpha}; \frac{\alpha+2}{\alpha}; -\frac{R_{\max}^\alpha}{2Kc\rho_{\text{r}}} \right) \right. \\ &\quad \left. - R_{\min}^2 {}_2F_1 \left( 1, \frac{1}{\alpha}; \frac{\alpha+2}{\alpha}; -\frac{R_{\min}^\alpha}{2Kc\rho_{\text{r}}} \right) \right\}. \end{aligned} \quad (70)$$

Similarly,  $\tilde{A}_2$  is expressed as

$$\begin{aligned} A_2 &\xrightarrow{a.s.} \tilde{A}_2 = K \mathbb{E}_{l_{k+K}} \left[ \left( \beta'_{k+K} \right)^{-1} \right] = \frac{K}{c} \int_{R_{\min}}^{R_{\max}} \left( \frac{1}{2K\rho_{\text{r}}c} \right. \\ &\quad \left. \times l_k^{2\alpha} + l_k^\alpha \right) f(l_k) dl_k = \frac{K}{c(R_{\max}^2 - R_{\min}^2)} \\ &\quad \times \left\{ \frac{1}{2K\rho_{\text{r}}} \frac{R_{\max}^{2\alpha+2} - R_{\min}^{2\alpha+2}}{c(\alpha+1)} + \frac{2(R_{\max}^{\alpha+2} - R_{\min}^{\alpha+2})}{\alpha+2} \right\}^2. \end{aligned} \quad (71)$$

Next, we will formulate  $\tilde{\mathcal{R}}(P_{\text{tx,R}}, K, M)$  relying on the LSF channel coefficients. According to (70) and (71), we have

$$\begin{aligned} \tilde{\mathcal{R}}(P_{\text{tx,R}}, K, M) &= \sum_{k=1}^K \min \left\{ \mathbb{E}_{l_1, \dots, l_K} \left[ \tilde{\mathcal{R}}_k^{(1)} \right], \right. \\ &\quad \left. \mathbb{E}_{l_1+K, \dots, l_2K} \left[ \tilde{\mathcal{R}}_k^{(2)} \right] \right\} = K \min \left\{ \tilde{\mathcal{R}}_k^{(1)}, \tilde{\mathcal{R}}_k^{(2)} \right\}, \end{aligned} \quad (72)$$

where

$$\begin{aligned} \tilde{\mathcal{R}}_k^{(1)} &= \mathbb{E}_{l_k} \left[ \log_2 \left( 1 + \frac{(M-K) P_{\text{tx,d}} \beta'_k}{P_{\text{tx,U}} \tilde{A}_1 + \sigma_{\text{R}}^2} \right) \right] \\ &= \int_{R_{\min}}^{R_{\max}} \log_2 \left( 1 + \frac{(M-K) P_{\text{tx,d}} \beta'_k}{P_{\text{tx,U}} \tilde{A}_1 + \sigma_{\text{R}}^2} \right) f(l_k) dl_k, \\ \tilde{\mathcal{R}}_k^{(2)} &= \mathbb{E}_{l_{k+K}} \left[ \log_2 \left( 1 + \frac{(M-K) P_{\text{tx,R}}}{\left( P_{\text{tx,R}} \tilde{\beta}_{k+K} + \sigma_{\text{D}}^2 \right) \tilde{A}_2} \right) \right] \\ &= \int_{R_{\min}}^{R_{\max}} \log_2 \left( 1 + \frac{(M-K) P_{\text{tx,R}}}{\left( P_{\text{tx,R}} \tilde{\beta}_{k+K} + \sigma_{\text{D}}^2 \right) \tilde{A}_2} \right) \\ &\quad \times f(l_{k+K}) dl_{k+K}. \end{aligned} \quad (73)$$

$\square$

APPENDIX III  
PROOF OF COROLLARY 2

According to the convexity of  $\log_2(1 + \frac{1}{x})$  and using Jensen's inequality, we obtain the following lower bound:

$$\begin{aligned} \tilde{\mathcal{R}}_k^{(1)} &= \mathbb{E}_{l_k} \left[ \log_2 \left( 1 + \frac{(M-K) P_{\text{tx,d}} \beta'_k}{P_{\text{tx,d}} \tilde{A}_1 + \sigma_{\text{R}}^2} \right) \right] \\ &\geq \log_2 \left( 1 + \frac{(M-K) P_{\text{tx,d}}}{P_{\text{tx,d}} \tilde{A}_1 + \sigma_{\text{R}}^2} \left( \mathbb{E}_{l_k} \left[ (\beta'_k)^{-1} \right] \right)^{-1} \right) \\ &\stackrel{(a)}{=} \log_2 \left( 1 + \frac{(M-K) K P_{\text{tx,d}}}{(P_{\text{tx,d}} \tilde{A}_1 + \sigma_{\text{R}}^2) \tilde{A}_2} \right) \triangleq \tilde{\mathcal{R}}_{\text{LB}}^{(1)}, \end{aligned} \quad (74)$$

where (a) is obtained by applying

$$\mathbb{E}_{l_k} \left[ (\beta'_k)^{-1} \right] = \mathbb{E}_{l_{k+K}} \left[ (\beta'_{k+K})^{-1} \right] = \frac{\tilde{A}_2}{K}. \quad (75)$$

Similarly, we have

$$\begin{aligned} \tilde{\mathcal{R}}_k^{(2)} &= \mathbb{E}_{l_k} \left[ \log_2 \left( 1 + \frac{(M-K) P_{\text{tx,R}}}{(P_{\text{tx,R}} \tilde{\beta}_{k+K} + \sigma_{\text{D}}^2) \tilde{A}_2} \right) \right] \\ &\geq \log_2 \left( 1 + \frac{(M-K) P_{\text{tx,R}}}{\tilde{A}_2} \left( P_{\text{tx,R}} \mathbb{E}_{l_{k+K}} \left[ \tilde{\beta}_{k+K} \right] + \sigma_{\text{D}}^2 \right)^{-1} \right) \\ &\stackrel{(b)}{=} \log_2 \left( 1 + \frac{(M-K) K P_{\text{tx,R}}}{(P_{\text{tx,R}} \tilde{A}_1 + K \sigma_{\text{D}}^2) \tilde{A}_2} \right) \triangleq \tilde{\mathcal{R}}_{\text{LB}}^{(2)}, \end{aligned} \quad (76)$$

where (b) is obtained by applying

$$\mathbb{E}_{l_{k+K}} \left[ \tilde{\beta}_{k+K} \right] = \mathbb{E}_{l_k} \left[ \tilde{\beta}_k \right] = \frac{\tilde{A}_1}{K}. \quad (77)$$

Substituting (74) and (76) into (72), we can readily obtain

$$\begin{aligned} \tilde{\mathcal{R}}(P_{\text{tx,R}}, K, M) &\geq K \min \left\{ \tilde{\mathcal{R}}_{\text{LB}}^{(1)}, \tilde{\mathcal{R}}_{\text{LB}}^{(2)} \right\} \\ &= K \tilde{\mathcal{R}}_{\text{LB}}(P_{\text{tx,R}}, K, M). \end{aligned} \quad (78)$$

According to (32), we have

$$\begin{aligned} \tilde{\eta}_{\text{EE}}(P_{\text{tx,R}}, K, M) &\geq \tilde{\eta}_{\text{EELB}}(P_{\text{tx,R}}, K, M) \\ &= \frac{(1 - \frac{2K}{T}) \frac{BK}{2} \tilde{\mathcal{R}}_{\text{LB}}(P_{\text{tx,R}}, K, M)}{P_{\text{tot}}(P_{\text{tx,R}}, K, M)}. \end{aligned} \quad (79)$$

□

REFERENCES

- [1] J. A. Stankovic, "Research directions for the internet of things," *IEEE Internet Things Journal*, vol. 1, no. 1, pp. 3–9, Feb. 2014.
- [2] A. Whitmore, A. Agarwal, and L. D. Xu, "The internet of things-A survey of topics and trends," *L. Inf Syst Front*, vol. 17, no. 4, pp. 261–274, Apr. 2015.
- [3] S. P. N. S. V. Shet, and C. K, "Energy efficient network architecture for IoT applications," in *Int. Conf. Green Comput. Internet Things (ICGCIoT)*, Noida, India, Oct. 2015, pp. 784–789.
- [4] R. Arshad, S. Zahoor, M. A. Shah, A. Wahid1, and H. Yu, "Green IoT: An investigation on energy saving practices for 2020 and beyond," *IEEE Access*, vol. 5, pp. 15 667–15 681, Jul. 2017.
- [5] X. Liu and N. Ansari, "Green relay assisted D2D communications with dual batteries in heterogeneous cellular networks for IoT," *IEEE Internet Things Journal*, vol. 4, no. 5, pp. 1707–1715, Oct. 2017.
- [6] R. Mahapatra, Y. Nijssure, G. Kaddoum, N. U. Hassan, and C. Yuen, "Energy efficiency trade-off mechanism towards wireless green communication: A survey," *IEEE Commun. Surveys & Tutorials*, vol. 18, no. 1, pp. 686–705, Jan. 2016.
- [7] Mckinsey Global Institute, "The internet of things: Mapping the value beyond the hype," June 2015, tech. Rep.
- [8] A. Gharaibeh, M. A. Salahuddin, S. J. Hussini, A. Khreishah, I. Khalil, M. Guizani, and A. Al-Fuqaha, "Smart cities: A survey on data management, security, and enabling technologies," *IEEE Commun. Surveys & Tutorials*, vol. 19, no. 4, pp. 2456–2501, Aug. 2017.
- [9] J. Zou, H. Yu, W. Miao, and C. Jiang, "Packet-Based preamble design for random access in massive IoT communication systems," *IEEE Access*, vol. 5, pp. 11 759–11 767, June 2017.
- [10] G. Hattab and D. Cabric, "Energy-Efficient massive cellular IoT shared spectrum access via mobile data aggregators," in *Proc. IEEE Int'l Conf. Pervasive Computing and Comm. (PERCOM)*, Rome, Italy, Oct. 2017, pp. 1–6.
- [11] M. Wang, W. Yang, J. Zou, B. Ren, M. Hua, J. Zhang, and X. You, "Cellular machine-type communications: Physical challenges and solutions," *IEEE Wireless Commun.*, vol. 23, no. 2, pp. 126–135, Apr. 2016.
- [12] H. Chaouchi, *The Internet of Things: Connecting Objects*. New York, USA: Wiley, 2010.
- [13] H. Thapliyal, V. Khalus, and C. Labrado, "Stress detection and management: A survey of wearable smart health devices," *IEEE Consumer Electronics Mag.*, vol. 6, no. 4, pp. 64–69, Oct. 2017.
- [14] 5G Americas, "LTE and 5G technologies enabling the internet of things," <http://www.5gamericas.org>, Bellevue, WA, USA, Dec. 2016.
- [15] Qualcomm Technologies, Inc., "Paving the path to narrowband 5G with LTE internet of things (IoT)," <http://www.qualcomm.com/5G>, San Diego, CA, USA, June 2016.
- [16] Z. Ding, L. Dai, and H. V. Poor, "MIMO-NOMA design for small packet transmission in the internet of things," *IEEE Access*, vol. 52, no. 2, pp. 1393–1405, Apr. 2016.
- [17] E. G. Larsson, O. Edfors, F. Tufvesson, and T. L. Marzetta, "Massive MIMO for next generation wireless systems," *IEEE Commun. Mag.*, vol. 52, no. 2, pp. 186–195, Feb. 2014.
- [18] R. Tian, Y. Liang, X. Tan, and T. Li, "Overlapping user grouping in IoT oriented massive MIMO systems," *IEEE Access*, vol. 5, pp. 14177–14 186, Jul. 2017.
- [19] J. Zuo, J. Zhang, C. Yuen, W. Jiang, and W. Luo, "Energy efficient user association for cloud radio access networks," *IEEE Access*, vol. 4, pp. 2429–2438, May 2016.
- [20] —, "Energy efficient downlink transmission for multi-cell massive DAS with pilot contamination," *IEEE Trans. Veh. Technol.*, vol. 66, no. 2, pp. 1209–1221, Feb. 2017.
- [21] H. Q. Ngo, E. Larsson, and T. Marzetta, "Energy and spectral efficiency of very large multiuser MIMO systems," *IEEE Trans. Commun.*, vol. 61, no. 4, pp. 1436–1449, Apr. 2013.
- [22] L. Lu, G. Y. Li, A. L. Swindlehurst, A. Ashikhmin, and R. Zhang, "An overview of massive MIMO: Benefits and challenges," *IEEE Journal Sel. Topics Signal Process.*, vol. 8, no. 5, pp. 742–758, May 2014.
- [23] S. Buzzi, C. L. I, T. E. Klein, H. V. Poor, C. Yang, and A. Zappone, "A survey of energy-efficient techniques for 5G networks and challenges ahead," *IEEE Journal Sel. Areas Commun.*, vol. 34, no. 4, pp. 697–709, Apr. 2016.
- [24] E. Bjornson, L. Sanguinetti, J. Hoydis, and M. Debbah, "Optimal design of energy-efficient multi-user MIMO systems: Is massive MIMO the answer?" *IEEE Trans. Wireless Commun.*, vol. 14, no. 6, pp. 3059–3075, Jun. 2015.
- [25] J. Joung, Y. K. Chia, and S. Sun, "Energy-efficient, large-scale distributed-antenna system (L-DAS) for multiple users," *IEEE Journal Sel. Topics Signal Process.*, vol. 8, no. 5, pp. 954–965, Oct. 2014.
- [26] W. Liu, A. Zappone, C. Yang, and E. Jorswieck, "Global EE optimization of massive MIMO systems," in *Proc. IEEE Int. Works. on Signal Process. Advances in Wireless Comm. (SPAWC)*, Stockholm, Sweden, Jun. 2015, pp. 221–225.
- [27] T. M. Nguyen, V. N. Ha, and L. B. Le, "Resource allocation optimization in multi-user multi-cell massive MIMO networks considering pilot contamination," *IEEE Access*, vol. 3, pp. 1272–1287, 2015.
- [28] H. A. Suraweera, H. Q. Ngo, T. Q. Duong, C. Yuen, and E. G. Larsson, "Multi-pair amplify-and-forward relaying with very large antenna arrays," in *Proc. IEEE Int. Conf. Commun. (ICC)*, Budapest, Hungary, Jun. 2013, pp. 1–6.
- [29] S. Jin, X. Liang, K.-K. Wong, X. Gao, and Q. Zhu, "Ergodic rate analysis for multipair massive MIMO two-way relay networks," *IEEE Trans. Wireless Commun.*, vol. 14, no. 3, pp. 1480–1491, Mar. 2015.

- [30] H. Q. Ngo, H. Suraweera, M. Matthaiou, and E. Larsson, "Multipair full-duplex relaying with massive arrays and linear processing," *IEEE Journal Sel. Areas Commun.*, vol. 32, no. 9, pp. 1721–1737, Sept. 2014.
- [31] M. Tao and R. Wang, "Linear precoding for multi-pair two-way MIMO relay systems with max-min fairness," *IEEE Trans. Signal Process.*, vol. 60, no. 10, pp. 5361–5370, Oct. 2012.
- [32] S. M. Kay, *Fundamentals of Statistical Signal Processing: Estimation Theory*. Upper Saddle River, NJ, USA: Prentice Hall, Mar. 1993.
- [33] J. Hoydis, S. ten Brink, and M. Debbah, "Massive MIMO in the UL/DL of cellular networks: How many antennas do we need?" *IEEE Journal Sel. Areas Commun.*, vol. 31, no. 2, pp. 160–171, Feb. 2013.
- [34] J. Joung and S. Sun, "EMA: Energy-efficiency-aware multiple access," *IEEE Commun. Lett.*, vol. 18, no. 6, pp. 1071–1074, Jun. 2014.
- [35] V. Gazis, "A survey of standards for machine-to-machine and the internet of things," *IEEE Commun. Surveys & Tutorials*, vol. 19, no. 1, pp. 482–511, July 2017.
- [36] A. Hu, T. Lv, H. Gao, Z. Zhang, and S. Yang, "An ESPRIT-based approach for 2-D localization of incoherently distributed sources in massive MIMO systems," *IEEE Journal Sel. Signal Process.*, vol. 8, no. 5, pp. 996–1011, Oct. 2014.
- [37] 3GPP TS 36.212, "Technical specification group radio access network; evolved universal terrestrial radio access (e-utra); multiplexing and channel coding (rel. 13)," Jun. 2016.
- [38] C. Pielli, A. Bion, A. Zanella, and M. Zorzi, "Joint optimization of energy efficiency and data compression in TDMA-based medium access control for the IoT," in *Proc. IEEE Globecom Workshops (GC Workshops)*, Washington, DC, USA, Dec. 2016, pp. 1–6.
- [39] W. Dinkelbach, "On nonlinear fractional programming," *Management Science*, vol. 13, no. 7, pp. 492–498, 1967.
- [40] K. T. K. Cheung, S. Yang, and L. Hanzo, "Achieving maximum energy-efficiency in multi-relay OFDMA cellular networks: A fractional programming approach," *IEEE Trans. Commun.*, vol. 61, no. 7, pp. 2746–2757, Jul. 2013.
- [41] S. Boyd and L. Vandenberghe, *Convex Optimization*. Cambridge, United Kingdom: Cambridge University Press, Mar. 2004.
- [42] Y.-U. Jang, E.-R. Jeong, and Y. H. Lee, "A two-step approach to power allocation for OFDM signals over two-way amplify-and-forward relay," *IEEE Trans. Signal Process.*, vol. 58, no. 4, pp. 2426–2430, Apr. 2010.
- [43] Z. Dawy, W. Saad, A. Ghosh, J. G. Andrews, and E. Yaacoub, "Toward massive machine type cellular communications," *IEEE Wireless Commun.*, vol. 24, no. 1, pp. 120–128, Feb. 2017.
- [44] R. Couillet and M. Debbah, *Random Matrix Methods for Wireless Communications*, 1st ed. Cambridge, United Kingdom: Cambridge University Press, Nov. 2011.
- [45] P. Billingsley, *Probability and Measure*, 2nd ed. New York: John Wiley Sons Inc., 1986.
- [46] A. van der Vaart, *Asymptotic Statistics (Cambridge Series in statistical and Probabilistic Mathematics)*, 1st ed. New York: Cambridge University Press, 1998.